



2020

## Biologically-Guided Isolation of Natural Lead Antithyroid Drug from *Medicago sativa* L. Sprouts and Its Toxic Profile in Comparison with Propylthiouracil

Follow this and additional works at: <https://www.jfda-online.com/journal>

 Part of the [Food Science Commons](#), [Medicinal Chemistry and Pharmaceutics Commons](#), [Pharmacology Commons](#), and the [Toxicology Commons](#)



This work is licensed under a [Creative Commons Attribution-Noncommercial-No Derivative Works 4.0 License](#).

### Recommended Citation

El-Mezayen, Nesrine S.; Khairy, Asmaa; Zaatout, Hala H.; Hammada, Hala M.; and Metwally, Aly M. (2020) "Biologically-Guided Isolation of Natural Lead Antithyroid Drug from *Medicago sativa* L. Sprouts and Its Toxic Profile in Comparison with Propylthiouracil," *Journal of Food and Drug Analysis*: Vol. 28 : Iss. 3 , Article 5.

Available at: <https://doi.org/10.38212/2224-6614.1242>

This Original Article is brought to you for free and open access by Journal of Food and Drug Analysis. It has been accepted for inclusion in Journal of Food and Drug Analysis by an authorized editor of Journal of Food and Drug Analysis.

# Biologically-Guided Isolation of Natural Lead Antithyroid Drug from *Medicago sativa* L. Sprouts and Its Toxic Profile in Comparison with Propylthiouracil

Reham S. Ibrahim<sup>a</sup>, Nesrine S. El-Mezayen<sup>b,\*</sup>, Asmaa Khairy<sup>a</sup>, Hala H. Zaatout<sup>a</sup>, Hala M. Hammuda<sup>a</sup>, Aly M. Metwally<sup>a</sup>

<sup>a</sup> Department of Pharmacognosy, Faculty of Pharmacy, Alexandria University, Alexandria, 21521, Egypt

<sup>b</sup> Department of Pharmacology, Faculty of Pharmacy and Drug Manufacturing, Pharos University in Alexandria, Alexandria, Egypt

## Abstract

Hyperthyroidism is a common endocrine disorder associated with increased risk of cardiovascular complications and mortality. Although antithyroid drugs (ATDs) are approved as first line option for many hyperthyroidism cases, including pregnancy and childhood, they exert significant toxic profile. *Medicago sativa* L. (alfalfa) also called “The father of all food” was among the diet consumed by mares that gave birth to foals with congenital hypothyroidism. Since, greenfeed was accused for the development of such condition, alfalfa may possess constituents with promising antithyroid potential that could be a valuable substitute for the conventional ATDs. The current work was designed to identify the most biologically active antithyroid phytoconstituent separated from alfalfa sprouts and comparing its antithyroid mechanism, efficacy and toxic profile to the standard ATD; propylthiouracil (PTU). The most biologically active solvent fractions from alfalfa sprouts extract were identified by *in vitro* screening for anti-thyroid peroxidase (TPO) activity, from which different phytoconstituents were separated and identified by interpretation of spectroscopic data. These compounds were then *in vitro* screened for anti-TPO and virtually screened via GLIDE XP docking into the crystal structures of the enzymes; bovine lactoperoxidase, as an alternative to TPO, and mammalian selenocysteine-dependent iodothyronine deiodinase (IDI), that are both uniquely dually prohibited by PTU. The compound that showed the least TPO IC<sub>50</sub> and highest combined docking XP score was elected for comparing its antithyroid mechanism, efficacy, tendency to reverse hyperthyroidism-triggered complications and toxicity to PTU using L-thyroxine-induced hyperthyroidism model in rats. Seven compounds (1–7) were isolated from the most biologically active fraction, whilst, compounds (4–7) were reported for the first time from alfalfa sprouts. Compound 5 (apigenin) showed the least TPO IC<sub>50</sub> and highest *in-silico* combined score, thus, apigenin was selected for further *in-vivo* investigations. Apigenin was found to more effectively interfere with type 1-IDI than with TPO *in vivo*. Apigenin therapy resulted in nearly euthyroid state, without incidence of hypothyroidism, thyroid hypertrophy, hepatotoxicity or WBCs count reduction. In addition, apigenin, but not PTU, corrected hyperthyroidism-induced left ventricular hypertrophy. Therefore, apigenin is a natural lead antithyroid drug that represents a possible safer alternative to conventional ATDs.

**Keywords:** Apigenin, hyperthyroidism, *Medicago sativa* L (alfalfa), thyroid peroxidase, type 1 iodothyronine deiodinase

## 1. Introduction

Since, thyroid gland hormones are crucial for normal cellular growth and metabolism, their imbalance is amongst the most common

endocrine disorders worldwide with overwhelming health consequences [1]. For instance, untreated hyperthyroidism is associated with increased risk of cardiovascular diseases, altered lipid profile, fractures and excess mortality [1, 2].

Received 13 April 2020; accepted 27 June 2020.  
Available online 28 August 2020.

\* Corresponding author. Department of Pharmacology, Faculty of Pharmacy and drug manufacturing, Pharos University, Alexandria, Egypt. Tel : 002 01111221955.  
E-mail address: sharabitarek@hotmail.com (N.S. El-Mezayen).

<https://doi.org/10.38212/2224-6614.1242>

2224-6614/© 2020 Taiwan Food and Drug Administration. This is an open access article under the CC-BY-NC-ND license (<http://creativecommons.org/licenses/by-nc-nd/4.0/>).

Among options for hyperthyroidism treatment are the antithyroid drugs (ATDs); such as propylthiouracil (PTU) and methimazole. ATDs are approved as a first line therapy for hyperthyroidism occurring in special patient populations such as; pregnancy, childhood, adolescence and for Grave's disease. These drugs are thionamide derivatives that share the ability to interfere with thyroid peroxidase (TPO)-mediated iodination of thyroglobulin tyrosine residues, a crucial step in the synthesis of thyroid hormones; thyroxine (T4) and triiodothyronine (T3). PTU possesses an additional ability to selectively interfere with type 1 iodothyronine deiodinases (IDI-1), responsible for the conversion of T4 to the active T3 within the thyroid and in peripheral tissues; liver and kidney [3, 4]. Unfortunately, significant toxic profile is documented to ATDs use; extreme risk of developing severe rapidly progressing liver damage with subsequent liver failure, obliging liver transplantation, is reported in most cases using ATDs. Besides agranulocytosis may develop which, though being quite low in frequency, is sudden in onset and life threatening [5]. Either experiencing side effects or the abrupt discontinuation of the ATDs can bring about lethal consequences [5, 6]. These facts highlight the urgent need for safer ATDs.

Since early 1980s, many sporadic cases of congenital hypothyroidism with hyperplastic goiter in newborn foals have been reported and documented in Canada, USA and Europe [7-13]. Research concerning the etiology of this condition excluded genetic causes [9], and suggested a major role of dietary consumption of greenfeed by pregnant mares [10, 13]. *Medicago sativa* L. (alfalfa) was among the greenfeed consumed by pregnant mares producing affected foals [7], suggesting that this herb may contain constituents with antithyroid potential. Alfalfa has been known since ancient times for its immense nutritional benefit and hence was referred to by ancients as “The father of all food” and nowadays by “The queen of forages” [14]. The abundance of valuable biologically active phytoconstituents in this herb encouraged its use in phytotherapy and folk medicine. For that reason, Alfalfa was named by the ancient Greeks “the medic grass” which is “herba medica” in Latin, then the name “Medicago” was given to this herb [15]. Sprouts (microgreens); edible germinated seeds harvested before true leaves development, are

picking up an eminent concern due to possessing higher concentrations of bioactive components and nutritional characteristics than mature greens [16, 17]. Alfalfa seedlings are well-known for their health-promoting phytoconstituents such as flavonoids, phenolic acids and saponins that exert broad spectrum of biological activities and protective mechanisms [18-20]. Sprouting of alfalfa is accompanied with increase in its phenolic content [21], and rapid biosynthesis of biologically active saponins [22]. Taken together, screening of alfalfa sprouts phytoconstituents for possible antithyroid potential may give rise to an efficient antithyroid therapy with safe profile.

Therefore, the current study aimed at screening different fractions produced by liquid-liquid fractionation of alfalfa sprout extract for *in vitro* TPO inhibitory activity. Identification of phytoconstituents separated from fractions with the most powerful TPO enzyme inhibition activity and evaluation of their antithyroid potential was another goal. The antithyroid potential of these isolated compounds was estimated by combined *in vitro* anti-TPO activity and *in silico* virtually-screened dual interaction with the biological targets of PTU; TPO and IDI-1. We also intended to test antithyroid efficacy and mechanism of action of the identified most biologically active compound, using animal model of hyperthyroidism, by assaying gene expression of thyroid-derived TPO and hepatic IDI-1, serum level of thyroid related hormones; thyroid stimulating hormone (TSH), thyroxine (T4) and triiodothyronine (T3) and thyroid gland histologic morphometric analysis. In addition, hyperthyroidism associated complications; dyslipidemia, by assaying serum cholesterol, HDL-cholesterol and triglycerides, and left ventricular hypertrophy (LVH), assessed by morphometric analysis of left ventricles histopathologically. Further, appraisal of hepatotoxicity and agranulocytosis development potential in comparison with PTU was another scope of the study.

## 2. Methods

### 2.1. Materials

Silica gel of 230-400 mesh size and precoated TLC plates (silica gel 60, GF-245) with adsorbent layer thickness 0.25 mm was obtained from E-Merck (Dramstadt, Germany). Sephadex LH-20 was purchased from Sigma-Aldrich (Munich, Germany). L-thyroxine (Eltroxin™) was from Aspen (Bad Oldesloe, Germany). PTU (Thyrocil®) was obtained from Amoun (Cairo, Egypt). Apigenin was

purchased from Sigma Aldrich (St.Louis, USA). Amplex™ Ultrared (AUR) was from Thermo Fisher (Massachusetts, United States). EZNA total RNA isolation kit was from Omega bio-tek, Norcross, United States. High capacity cDNA reverse transcription kit, SYBR® green PCR master mix and SYBR® green RT-PCR reagents kit were from Applied Biosystems (California, United States). T4, T3 and TSH Fluorometric Enzyme Immunoassay (FEIA) assay kits were from Tosoh (Tokyo, Japan). Alanine aminotransferase (ALT) and aspartate aminotransferase (AST) colorimetric assay kits were purchased from N.S. Bio-Tec (Cairo, Egypt). Triglycerides, total cholesterol and HDL-cholesterol biochemical assay kits were from Biosystems (Barcelona, Spain). Other used chemicals were of analytical grade.

## 2.2. Animals

The present study was conducted on 40 healthy female Sprague Dawley rats of a locally bred strain, weighing  $200 \pm 10$  g each. The rats were purchased from and housed in animal house of Faculty of Pharmacy, Pharos University in Alexandria (PUA) (Alexandria, Egypt) under standard environmental conditions. They were permitted to acclimatize for a minimum of one week prior to experimentation. Use of animals and experimental procedures were approved by the Ethics Committee, Faculty of Pharmacy, PUA in fulfillment of The NIH Guide for the Care and Use of Laboratory Animals [23].

## 2.3. Extraction and Isolation of Biologically-Active Components of *Medicago sativa* L. Sprouts

### 2.3.1. Sprouting of *M. sativa* seeds

1.7 Kg of *M. sativa* seeds (obtained from Agricultural Research Centre, Cairo University, Egypt). A voucher sample of the seeds was kept at Pharmacognosy Department, Faculty of pharmacy, Alexandria University (Voucher sample number RS001). The seeds were washed with deionized water, sterilized using 5% sodium hypochlorite, drained and then washed with buffered water at pH 7. The seeds were then soaked in the buffered water for four hours, transferred to biochemical incubator (Shel Lab, Sheldon Mfg. Inc., USA) over a layer of moist filter papers and allowed to germinate under dark conditions at 22 °C for eleven days. The sprouts were kept moist by spraying sterile water by mist generator twice daily.

### 2.3.2. Identification of the alfalfa sprouts fractions with highest *in vitro* antithyroid potential

**2.3.2.1. Preparation of alfalfa sprouts extract solvent fractions.** The sprouts of the eleventh day were air-dried, powdered, soaked twice in 5.5 L EtOH (70%) each for 12 days at room temperature and then filtered. The combined filtrate was concentrated under reduced pressure to yield the extract (150 g). The extract was distributed in 30% MeOH then partitioned with petroleum ether, methylene chloride, ethyl acetate and n-butanol, sequentially.

**2.3.2.2. *In vitro* TPO inhibition assay.** TPO activity was assayed using amplex ultraRed assay as described earlier by Dong et al., with slight modifications [24]. Briefly, thyroid glands from 8 rats were homogenized in extraction buffer composed of 5 mM potassium phosphate buffer (pH 7), 200 mM sucrose, 1 mM EDTA and catalase 500 U/ml, then, centrifuged for 10 min at 4000 rpm. Supernatants were centrifuged, without catalase addition, at 15,000 rpm at 5°C for 5 min using cooling-centrifuge (Centurion-scientific-K3series, UK). Bradford protein assay kit (Bio-Basic Inc., Ontario, Canada) was used for protein quantification according to manufacturer's instruction. Five  $\mu$ L of thyroid extract was added to opaque well plates containing 10 mM of AUR and different plant extract fractions (total volume 200  $\mu$ L). For each fraction, four different final concentrations (0.2, 0.4, 0.8, 1 and 2 mg/mL) in triplicates using PTU as a reference standard at concentrations of 12.5, 25, 50, 100 and 200  $\mu$ g/mL. Hydrogen peroxide (0.3%) was added, plates were shaken in dark for 30 min then fluorescence was quantified at 544/590 nm excitation/emission using a PerkinElmer HTS7000 Bio Assay Reader (Norwalk, USA). Determination of IC<sub>50</sub> was done by interpolation of dose-response curves using GraphPad Prism, version 6.00. IC<sub>50</sub> values were calculated at fitted models, based on a dose-dependent mode of action, as the concentration of the tested compound that gave 50% of the maximum inhibition.

### 2.3.3. Biologically-guided isolation of alfalfa sprouts phytoconstituents with antithyroid potential

Since the two fractions with the least TPO IC<sub>50</sub> were the methylene chloride and ethyl acetate fractions, they were the only fractions subjected to column chromatography to yield subfractions from

which different phytoconstituents were separated, identified and screened for *in vitro* TPO inhibitory action.

The CH<sub>2</sub>Cl<sub>2</sub> fraction (5 g) was applied to silica gel column chromatography and eluted with a CH<sub>2</sub>Cl<sub>2</sub>–MeOH gradient solvent (100:0 - 93:7) to afford three fractions (A, 0.5 g; B, 0.9 g; C, 0.7 g). Fraction A was separated by preparative TLC on pre-coated plates using Hexane– Ethyl acetate (8:2) as the developing system. The band of (R<sub>f</sub> = 0.51) was scraped off and eluted with a mixture of CH<sub>2</sub>Cl<sub>2</sub>–MeOH (1:1) to afford compound 1 (9 mg). Fractions B and C were separately subjected to isocratic elution on sephadex LH-20 column using methanol to afford compound 2 (8.5 mg) from fraction B, and compound 3 (9.5 mg) from fraction C.

The EtOAc fraction (3.1 g) was applied to silica gel column chromatography and eluted with a CH<sub>2</sub>Cl<sub>2</sub>–MeOH gradient solvent (95:5 - 70:30) to obtain four fractions (D, 0.4 g; E, 0.2 g; F, 0.5 g; G, 0.1 g). Fraction D was chromatographed on sephadex LH-20 column to afford compound 4 (10.5 mg). Fraction E was similarly treated as fraction D to afford compound 5 (9.2 mg). Fraction F yielded compound 6 (12 mg) upon crystallization. Fraction G was applied to silica gel column chromatography and eluted with EtOAc– MeOH– H<sub>2</sub>O gradient solvent (120:5:4 - 45:5:4) to afford compound 7 (11.5 mg).

Identification of the isolated compounds was done using nuclear magnetic resonance analyses (<sup>1</sup>H-NMR, <sup>13</sup>C-NMR, COSY, HMQC, and HMBC); using TMS as a reference standard; were recorded on Varian AS spectrometer; at 400 MHz (<sup>1</sup>H) and 100 MHz (<sup>13</sup>C).

IC<sub>50</sub> for TPO of the separated compounds were subsequently calculated, as mentioned earlier, at concentrations of 12.5, 25, 50, 100 and 200 µg/mL as triplicates *versus* PTU.

#### 2.4. *In-silico* Virtual Screening of Phytoconstituents Derived from the Most Biologically-Active *M. Sativa* L. Sprouts Fractions

Compounds separated from alfalfa biologically active fraction were virtually screened for interaction with TPO and iodothyronine deiodinase in comparison with PTU. The compound with the highest virtual combined binding score for both enzymes and *in vitro* anti-TPO activity will be promoted for *in vivo* studies.

##### 2.4.1. Hardware setup and molecular docking

All prediction and processes were performed on an Intel i7-core workstation with 2.5 + GHz, 8 GB of RAM, and a high-end RADEON graphical processing unit. All programs were run on the Windows 10 Pro platform. Molecular docking was performed using Schrodinger Maestro 9.1 software package (LLC, New York, NY).

##### 2.4.2. Ligands preparation

The structures of compounds 1–7 were drawn using ChemDraw® Professional software 17.1. (PerkinElmer's). The structures were saved as (.Mol) files. Ligands were optimized and energetically minimized through OPLS 3 force field algorithm embedded in the LigPrep module of Schrödinger suite. The ionization states of the ligands were predicted at pH 7 ± 2 and Epik tool was selected to generate tautomers. Ligands were then desalted and specified chiralities were retained. Structures of unidentified stereochemistry are automatically subjected to all possible conformational changes for selection of best pose. The optimized structures were saved as maestro format (.mae) to retain 3D conformers.

##### 2.4.3. Protein structure preparation

X-ray crystal structures of bovine lactoperoxidase (4gn6) and mammalian selenocysteine dependent IDI-1 (PDB ID: 4tr3) were imported (as .pdb file) from the RCSB Protein Data Bank (PDB) (<http://www.rcsb.org/>). Preparation of 4tr3 structure and 4gn6 structures was performed using the PrepWiz module implemented in Schrodinger suite. The protein was first preprocessed where bond orders were assigned. All the water molecules beyond 5 Å from the active site were deleted. Hydrogen bonds were assigned using PROPKA function at PH 7. Finally, energy was minimized using OPLS 3 force field. For grid generation; the amino acid residues involved in iodothyronine binding were selected [25], while for 4gn6 the grid was generated from the residues involved in the interaction with the co-crystallized ligand [26].

##### 2.4.4. Molecular docking of the prepared ligands

The prepared ligands were flexibly docked using GLIDE docking with extra precision (XP) mode. Maestro interface was implemented to investigate the 2D and 3D interactions between the docked

ligands and the target such as hydrogen bonding, ion-pairing and hydrophobic interactions.

## 2.5. Experimental Design for the *in-vivo* Studies

Apigenin was found to be the compound with the least TPO IC<sub>50</sub> and highest *in silico* binding score for TPO and IDI-1 and hence was promoted to *in vivo* studying.

### 2.5.1. Experimental grouping and sampling

Hyperthyroidism was induced in 24 rats using L-thyroxine at a dose of (600 µg/kg) orally for fourteen successive days [27]. These rats were randomly assigned to one of these three groups (each comprised 8 rats): Positive control rats that did not receive any treatment (L-thyroxine + no treatment). PTU-treated (L-thyroxine + PTU) group; rats received 10 mg/kg PTU intra-peritoneal injection (i.p.) for 21 successive days [28], and apigenin-treated (L-thyroxine + apigenin) group; rats received apigenin orally for 21 successive days (dose was selected according to a pilot study results). Positive control group and other treated groups were compared to 8 plain normal control rats that received 1 mL distilled water orally for 14 successive days.

At the end of treatment period, rats were anesthetized, and blood samples were withdrawn from retro orbital venous plexus using capillary hematocrit tube. Part of blood samples was collected in EDTA-coated tubes for white blood cells counting. Another part was collected in tubes containing clot activator for sera separation by centrifugation at 3000 rpm for 15 minutes for assaying thyroid gland related hormones (T3, T4 and TSH), liver function tests (ALT and AST), and dyslipidemia markers; triglycerides, Cholesterol and HDL-cholesterol. After that, animals were sacrificed, then, thyroid glands and livers were quickly isolated, divided into halves; half was snap frozen in liquid nitrogen for RT-PCR assays and the other half was kept in 10% formal-saline for routine H&E staining. Hearts were also separated and left ventricles were carefully detached, blotted and weighed, for the assessment of LVH, then kept in 10% formal-saline for staining with H&E and Masson's trichrome (specific stain for fibrous tissue) for subsequent histopathological examination and morphometric analysis.

### 2.5.2. Evaluation of the antithyroid potential of apigenin versus PTU *in-vivo*

2.5.2.1. RNA isolation quantitative RT-PCR (qPCR) assay of TPO and IDI-1. The thyroid gland and

hepatic expression of TPO and IDI-1 was performed using two step qRT-PCR according to MIQE guidelines. Total RNA was isolated using the EZNA total RNA isolation kit (Omega bio-tek, Norcross, United States) according to manufacturer's instructions. The concentration and purity of RNA were determined spectrophotometrically by measuring absorbance at 260 and 280 nm. The A260/A280 ratio of 1.8-2.0 corresponds to 90%-100% pure nucleic acid. The cDNA was generated using 2 µg of total RNA in a total volume of 20 µL by reverse transcription (High capacity cDNA reverse transcription kit; Applied Biosystems, California, United States). The cDNA is then amplified using IDI-1 primer (forward sequence; 5'-TTAGTCCA-TAGCAGATTTTCTTGTC-3' and reverse sequence; 5'-CTGATGTCCATGTTGTTCT-TAAAAGC-3'), TPO primer (forward sequence; 5'-GTTGTTGCAAGCTCCTGTGA-3' and reverse sequence; 5'-GCCTTCTCCCCTTCATCTC-3') and GAPDH reference gene (forward sequence; 5'-GACAACCTTGGCAGTGGGA-3' and reverse sequence; 5'-ATGCAGGGATGATGTTCTGG-3'). This was performed by qRT-PCR using SYBR® Green PCR master mix and SYBR® green RT-PCR reagents kit (Applied Biosystems, California, United States) according to manufacturer's instructions. The data acquisition was collected during the extension step using Rotor-Gene Q-Pure detection, software version 2.1.0 (build 9); Qiagen, Hilden, Germany. The relative expression of target genes was quantified relative to the expression of the reference gene in the same sample and expressed as normalized ratio. This was done by calculating the threshold cycles (Ct) values of target genes to that of the reference using  $\Delta\Delta C_t$  method [29].

2.5.2.2. Assessment of T3, T4 and TSH serum levels. Serum level of T3, T4 and TSH was quantified using FEIA assay kits based on competitive enzyme immunoassay according to manufacturer's instructions [30].

2.5.2.3. Evaluation of thyroid glands function via histologic morphometric analysis. Formal saline-fixed thyroid glands samples were dehydrated and then paraffin-embedded. Sections (3-4 µm) were cut, deparaffinized, hydrated using descending grades of alcohol and then stained by H & E stain. Each stained section was examined by an investigator blinded to the experimental group using light microscope (Inverted Microscope ECLIPSE Ti-S, Nikon, Japan). The mean cross thickness of follicular lining epithelium, as indicator of thyroid activity, was measured in twenty follicles (10 from

Table 1. TPO IC<sub>50</sub> of different alfalfa sprout extract fractions, separated compounds from the most biologically active fractions and of PTU.

Extract Fraction	IC <sub>50</sub> (mg/mL)	Separated Compound	IC <sub>50</sub> (µg/mL)
Petroleum ether	NA	—	—
Methylene chloride	1.78 ± 0.24	Spinasterol	NA
		Liquiritigenin	84.37 ± 1.34
		Isoliquiritigenin	76.55 ± 3.87
Ethyl acetate	1.67 ± 0.85	4',7-dihydroxyflavone	112.04 ± 5.47
		Apigenin	41.07 ± 1.2
		Medicarpin-3-O-β-D-glucoside	NA
		Medicagenic acid-3-O-β-D-glucopyranoside	NA
n-butanol	NA	—	—
PTU			42.67 ± 3.45

All measurements were done in triplicates and expressed as mean ± SD. (NA: not applicable; the compound did not produce an inhibition curve, PTU: propylthiouracil).

peripheral zone and 10 from central zone) from each rat thyroid gland sections for all groups using ImageJ software [28].

### 2.5.3. Assessment of hyperthyroidism-associated dyslipidemia

Serum triglycerides [31], total cholesterol [32], and HDL-cholesterol [33] were assayed quantitatively by spectrophotometric methods using UV spectrophotometer (UV-1800, Shimadzu, Japan) according to their biochemical assay kits instructions.

### 2.5.4. Assessment of hyperthyroidism-associated LVH

LVH was assessed by measuring wet left ventricle weight (LVW) in milligrams and calculating the percentage of the ratio of LVW in milligrams to total rat body weight (BW) in grams (LVW/BW in mg/g) [34].

Further assessment of LVH was done via morphometric analysis histopathologically; Sections were prepared as mentioned before. The cardiomyocyte width of 50 cells per each H&E stained sections of left ventricle samples was measured under magnification of 400 using ImageJ software. The width was measured passing through the center of the nucleus. Only myocytes with longitudinal circular midwall muscle bundles were considered.

To identify possible interstitial fibrosis, other sections were stained by the Masson's trichrome stain to identify collagen fibers. The amount of collagen fibers was quantified by analyzing the amount of blue color in each left ventricle tissue section using ImageJ software [34,35].

## 2.6. Comparing Toxicities Associated With Antithyroid Therapies

### 2.6.1. Evaluation of hepatotoxicity biochemically and histopathologically

ALT and AST were assayed in sera obtained from all rats of different groups colorimetrically

according to instructions provided by their kits' suppliers [35, 36].

Further evaluation of hepatotoxicity was performed via histopathologic examination of H&E stained liver tissue sections. As an indication of liver damage, the mean width of 20 sinusoidal spaces from each rat liver tissue sections for all groups was measured using imageJ software [28].

### 2.6.2. Assessing the potential of developing agranulocytosis

This was performed by counting the number of white blood cells per cubic centimeter of blood.

## 2.7. Statistical Analysis of the Data

Data were fed and analyzed using IBM SPSS software package version 20.0. (Armonk, NY: IBM Corp) [37]. The Kolmogorov-Smirnov test was used to verify the normality of distribution. Quantitative data were described using mean and standard. For normally distributed quantitative data comparisons among the different groups were done using analysis of variance (ANOVA; F test) followed by a Post Hoc test (Games-Howell) for pair wise comparison. Significance of the obtained results was judged at the 5% level [38].

## 3. Results and discussion

The profound toxicity associated with ATDs, highlights the need for alternative and safer anti-thyroid medication [5]. Since alfalfa was among herbs suspected for developing congenital hypothyroidism in mares [10, 13], it may possess phytoconstituents with combined efficient antithyroid activity and safe profile. Alfalfa microgreens captured great interest in recent years for showing higher concentrations of the valuable phytochemicals than mature ones [16, 17]. Thus, screening alfalfa microgreens for a possible ATD may be of value

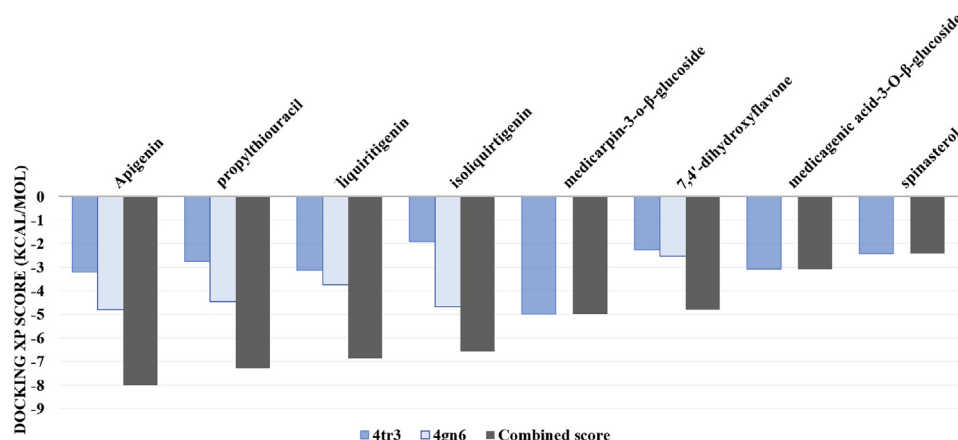


Fig. 1. Extra-precision (XP) scores in (Kcal/mol) of the docked compounds in to the crystalline structures of lactoperoxidase (4gn6), IDI-1 (4tr3) and the combined scores for both enzymes.

especially if this drug revealed safer profile than the standard ATD; PTU.

### 3.1. Biologically-Guided Isolation of Alfalfa Sprouts Phytoconstituents with Antithyroid Potential

The antithyroid potential of all solvent fractions derived from alfalfa sprouts extract were evaluated by calculating  $IC_{50}$  for TPO (Table 1). Among the four fractions, the methylene chloride and ethyl acetate fractions showed TPO inhibitory potential and thus were chosen for further analysis. Three subfractions with three different phytoconstituents (compounds 1-3) and four subfractions with three different phytoconstituents (compounds 4-7) were separated from the methylene chloride and ethyl acetate fraction, respectively.

Based on  $^1H$  NMR, APT, HMQC, HMBC and COSY spectral analyses, supplementary (Tables T1-T4) and (Fig. S1-S35); compounds (1–7) were identified as spinasterol (1) [39, 40], liquiritigenin (2), isoliquiritigenin (3) [41-43], 4',7-dihydroxyflavone (4) [44], apigenin (5) [45], medicarpin-3-O-β-D-glucoside (6) [46], and medicagenic acid-3-O-β-D-glucopyranoside (7) [47]. It is worthy to mention that compounds (4–7) were reported for the first time from the sprouts of alfalfa.

The *in vitro* TPO inhibitory activity of the seven identified compounds was compared to that of PTU. Among the seven tested compounds, apigenin (compound 5) demonstrated the highest *in vitro* anti-TPO activity ( $IC_{50}$ :  $41.07 \pm 1.2$ ) that was very close to that of PTU, Table 1.

### 3.2. In-Silico Virtual Screening of Phytoconstituents Derived From the Most Biologically-Active M. Sativa L. Sprouts Fractions

Two molecular targets were selected for *in silico* virtual screening of the seven separated compounds; TPO, the main target for all ATDs, and selenocysteine dependent IDI-1, an exclusive target for PTU that is responsible for activation of T4 to produce T3 within the thyroid and in peripheral tissues [5]. Since lactoperoxidase (LPO) has a well-characterized crystal structure and shares structural homology with TPO, it is usually used for studying drug-TPO interaction [48, 49]. In the current study, we imply selenocysteine dependent IDI-1 (PDB ID: 4tr3) and LPO (4gn6) for virtual screening.

Compounds (1–7) were separately docked using extra-precision (XP) glide docking into the active binding pockets of (4tr3) and (4gn6). Fig. 1 shows the results of the molecular-docking simulation performed using the 3D structures of compounds (1–7) and of PTU on the two selected molecular targets, together with the combined score. This combined score gives an insight of a possible equipotency of the test compound to PTU.

The simulated molecular docking showed that the highest combined binding score for both enzymes was attained by apigenin. Apigenin possessed considerable binding affinity to both targets; 4tr3 and 4gn6 with XP scores  $-3.2$  and  $-4.8$ , respectively. In comparison with PTU, apigenin had higher binding affinity for 4tr3 (IDI-1) but very close affinity to 4gn6 (LPO). This indicates that the observed higher combined score of apigenin compared to

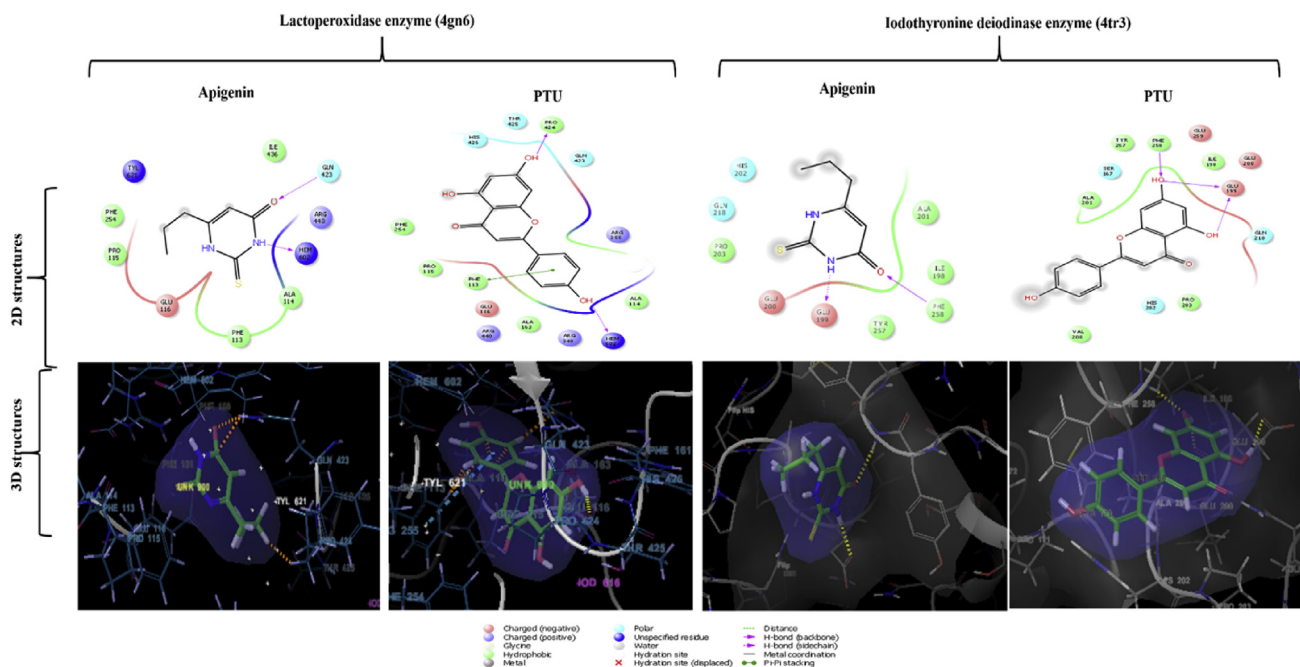


Fig. 2. 2D and 3D interaction diagrams of propylthiouracil and apigenin with lactoperoxidase (4gn6) and IDI-1 enzyme (4tr3).

PTU is due to its possible higher inhibitory activity towards IDI-1. Medicarpin-3-*O*- $\beta$ -D-glucoside has the highest score for 4tr3 binding, however, it totally lacked binding affinity towards the primary target of ATDs; 4gn6.

The interactions between apigenin, PTU and the two target enzymes were analyzed, Fig. 2. Structural representations of the best conformation of the complexed active site of LPO (4gn6) with apigenin and PTU revealed that both of them could successfully interact with heme group which is essential for the activity [48]. As shown in Fig. 2, apigenin is inserted deeply in the cavity, interacting with binding pocket amino acid residues Glu 116 and Pro 424 through ionic and H-bond contacts, respectively. In addition to Pi-Pi stacking with Phe 113 and many other hydrophobic and polar interactions. PTU unveiled less interactions in the binding cavity (Fig. 2).

Apigenin interacts via different modes with numerous amino acid residues present in the catalytic domain of selenocysteine-dependent IDI-1 (4tr3) as evidenced from Fig. 2. The 5-hydroxyl group of apigenin formed a hydrogen bond with the side chain of Glu199 while the 7-hydroxy engaged with two hydrogen bonds with the backbones of Glu199 and Phe258. Polar interactions were also

observed with Ser176, His202 and Gln218. In addition to numerous hydrophobic contacts with Ile198, Ala201, Pro203, Val208, Tyr257, Phe258 and charged negative interactions with Glu200 and Glu259. Whereas, PTU exhibited notably fewer interactions in the binding domain, namely; two hydrogen bonds with Glu 199, Phe 258; polar interactions with His202, Gln218; charged negative interaction with Glu199, Glu200 and hydrophobic interactions with Ile198, Ala201, Pro203, Tyr257 and Phe258.

### 3.3. Evaluation of Antithyroid Potential of Apigenin versus PTU *in-vivo*

#### 3.3.1. Antithyroid mechanism prediction

In order to conclude the exact antithyroid mechanism of apigenin *in vivo*, gene expression of the ATDs' targets; thyroidal TPO and hepatic IDI-1, were quantitatively assessed using qrt-PCR technique following 21 days of treatment administration. It was evident from this experiment that both PTU and apigenin therapies markedly decreased gene expression of both targets compared to positive control rats. However, TPO expression was significantly less in PTU-treated group than in apigenin-treated group, while hepatic IDI-1 expression was significantly less in apigenin-treated group (Fig. 3A).

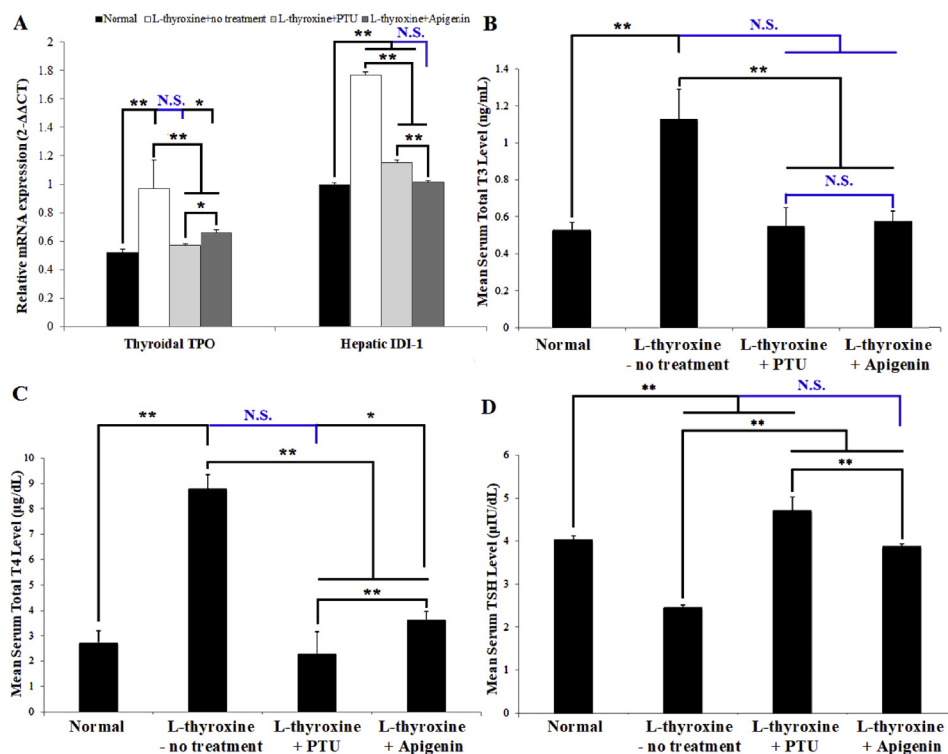


Fig. 3. The effect of apigenin and PTU on thyroidal TPO, hepatic IDI-1 expression and thyroid related hormones levels. A: mRNA expression of thyroidal TPO and hepatic IDI-1; B-D: serum T3, T4 and TSH, respectively. ANOVA test was used to compare between the different groups with Post Hoc Test (Tukey).\*: Statistically significant at  $p \leq 0.05$ , \*\*: Statistically significant at  $p \leq 0.001$ , N.S: Statistically non-significant ( $p > 0.05$ ),  $2^{-\Delta\Delta C_t}$ : normalized expression ratio,  $n = 8$ ; all results are presented as mean  $\pm$  SD. (PTU: propylthiouracil, TPO: thyroid peroxidase, IDI-1: type 1 iodothyronine deiodinase, T3: triiodothyronine, T4: thyroxine and TSH: thyroid stimulating hormone).

The observation regarding TPO expression contradicts our *in silico* and *in vitro* results that revealed higher affinity and binding score and less  $IC_{50}$  for TPO of apigenin than PTU. It can be inferred that pharmacokinetics of both therapies play a major role in their effect on TPO *in vivo*; as PTU is mainly distributed and concentrated in thyroid gland tissue and less to hepatic tissue [26], whereas apigenin is preferably distributed to small intestine and liver than other tissues [50]. These results indicate that apigenin is more active against IDI-1 than TPO *in vivo*.

### 3.3.2. Effect on thyroid gland related hormones (T3, T4 and TSH) serum levels

With the purpose of confirming apigenin antithyroid mechanism and subsequent antithyroid efficacy, serum levels of thyroid related hormones were assayed using FEIA technique. In the present study, apigenin therapy resembled PTU therapy in significantly decreasing serum T3 and T4 levels and

increasing TSH level compared to those observed with untreated rats with induced hyperthyroidism ( $p < 0.001$ ) (Fig. 3). Upon comparing hormones level following apigenin and PTU therapies, PTU-treated group had significantly less serum T4 levels signifying powerful inhibition of TPO by PTU more than apigenin *in vivo*. These results further confirm the ability of apigenin to selectively interfere with the peripherally acting enzyme; IDI-1 (which is responsible for production of active T3 and consequent feedback decrease in TSH level), more than with thyroidal TPO (responsible for T4 production). The non-significant difference in serum T3 level between PTU and apigenin-treated groups verifies the powerful IDI-1 inhibition by apigenin that compensated for its less efficacy against TPO *in vivo*.

Regarding effect of both therapies on serum TSH level, apigenin therapy was able to almost achieve euthyroid state, as apparent from the normalization of TSH level. On the other hand, PTU therapy resulted in significant elevation of TSH compared to

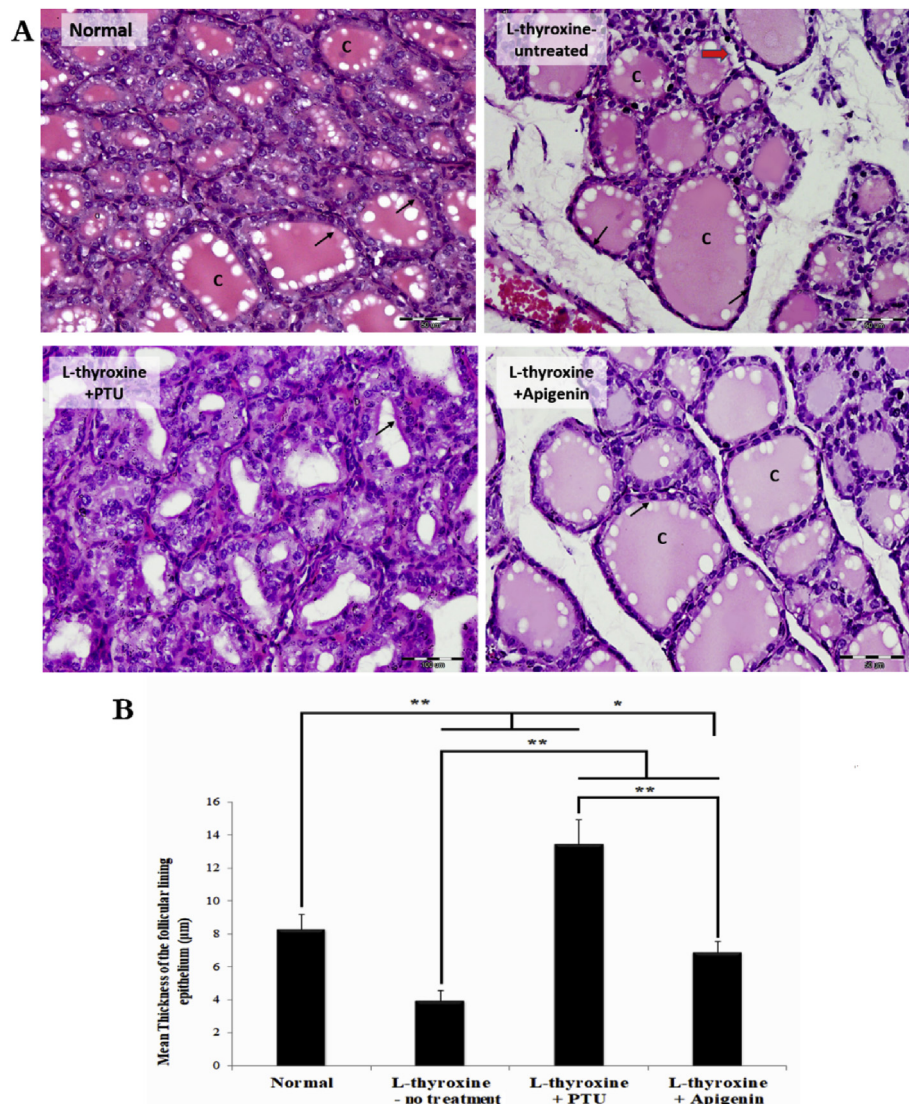


Fig. 4. Effect of different therapies on thyroid gland histology. A; H&E-stained thyroid gland tissue sections obtained from rats of different groups. B; Quantitative analysis of the thickness of thyroid gland follicular lining epithelium. All images were captured under magnification power  $\times 400$ . Black arrows point to the lining epithelium of the follicles, Red arrow points to scalloping in colloid (C: colloid). The mean cross thickness of follicular lining epithelium was measured in twenty follicles in thyroid gland sections obtained from each rat for all groups using ImageJ software. ANOVA test was used to compare between the different groups with Post Hoc Test (Tukey).\*: Statistically significant at  $p \leq 0.05$ , \*\*: Statistically significant at  $p \leq 0.001$ , N.S: Statistically non-significant ( $p > 0.05$ ),  $n = 8$ ; all results are presented as mean  $\pm$  SD.

normal rats indicating possible occurrence of sub-clinical hypothyroidism, as a side effect, emphasizing the importance of thyroid hormone monitoring and subsequent PTU dose adjustment during therapy [4, 5].

### 3.3.3. Evaluation of thyroid glands function via histologic morphometric analysis

In view of the fact that the thickness of the follicular epithelium and colloid morphology correlate to

the thyroid's functional status [51], H&E-stained thyroid glands tissue sections of different groups were examined and follicular size and its lining epithelial thickness were quantitatively assessed. Examination of thyroid glands sections obtained from normal rats revealed normal histological appearance; follicles appear lined by simple low cuboidal epithelium with homogenous colloid including some endocytotic vacuoles found near the margin of colloid filled lumen. Contrariwise, some

follicles of positive control rats appear lined with almost flat cells with relatively less vacuoles with frequently observed scalloping colloid, Fig. 4. These observed histopathologic changes indicate successful induction of hyperthyroidism [52]. Quantification of the follicular lining epithelium thickness demonstrates significant reduction in thickness in rats with induced hyperthyroidism compared to normal rats further confirming incidence of hyperthyroidism.

PTU therapy resulted in hyperplasia; increased cell number, and hypertrophy; increased cell size and colloid depletion. Follicles are lined with high cuboidal cells with significantly larger thickness compared to those of normal rats. PTU ability to induce hyperplasia and hypertrophy as a result of the increased production of thyrotrophic hormone and thyroid hypoactivity is the reason for developing benign and metastatic tumors in the thyroid gland upon prolonged administration [53]. These morphological alterations further intensify the need for safer alternative therapy. On the other hand, thyroid gland sections of rats treated with apigenin showed significant increase in thyroid lining epithelium thickness compared to those obtained from positive control rats. Moreover, the mean epithelial thickness was not significantly different from that of normal rats. There were many vacuoles in the uniform colloid which is a sign of decreased thyroid activity [52], which was confirmed by occasional observation of scalloping colloid. It is noteworthy to mention that the histopathological examination results impressively matched our biochemical findings.

#### 3.4. Evaluation of Hyperthyroidism-Associated Dyslipidemia

Since thyroid dysfunction have prominent effect on lipid profile, we compared the effect of the tested antithyroid medications on the altered lipid profile. Results of the present work revealed that serum samples of positive control rats had significantly higher TG concentration ( $p = 0.023$ ) and significantly less cholesterol and HDL-cholesterol than those of normal rats ( $p > 0.001$ ), Fig. 5. Former reports regarding altered triglycerides level in association with hyperthyroidism are conflicting; in agreement with our results some studies confirmed triglycerides elevation in patients with hyperthyroidism as well as in experimentally induced hyperthyroidism [27, 54, 55]. A possible explanation for this is the increased energy expenditure and hepatic

lipogenesis accompanying hyperthyroidism, most probably, due to boosted gene expression of lipogenesis genes [54]. On the contrary, some studies reported that triglycerides level is not affected by hyperthyroidism due to compensatory mechanisms [56, 57].

On the other hand, our results concerning decreased cholesterol and HDL-cholesterol levels as a result of hyperthyroidism are in agreement with previous studies [27, 57, 58]. The depressed level of these lipids can be explained by the ability of thyroid hormones increase LDL receptors gene expression that increases cellular uptake of LDL-cholesterol from circulation resulting in decreased levels of circulating total cholesterol [58]. In addition, hyperthyroidism related increase in free T4 level can enhance LDL oxidability. Moreover, high level of thyroid hormones can stimulate lipoprotein lipase activity leading to decreased circulating levels of lipoproteins [58]. Furthermore, this elevated level of thyroid hormones modify HDL-cholesterol metabolism by increasing transfer of cholesteryl esters from HDL to very low density lipoproteins [57, 58].

Administration of PTU and apigenin therapies for 3 successive weeks showed significant decrease in the serum TG concentration and significant increase in serum cholesterol and HDL-cholesterol as

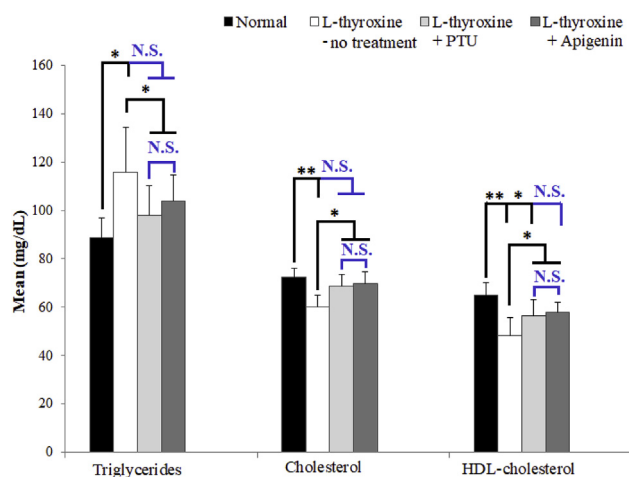


Fig. 5. Effect of different therapies on lipid profile of rats with induced hyperthyroidism. ANOVA test was used to compare between the different groups with Post Hoc Test (Tukey).\*: Statistically significant at  $p \leq 0.05$ , \*\*: Statistically significant at  $p \leq 0.001$ , N.S.: Statistically non-significant ( $p > 0.05$ ),  $n = 8$ ; all results are presented as mean  $\pm$  SD.

compared to untreated group. Except for HDL-cholesterol, where serum samples of PTU-treated group showed significantly less concentration compared to those obtained from normal rats, there was no statistically significant difference between PTU-treated, apigenin-treated and normal control groups regarding all tested lipid profile parameters, Fig. 5. Since the tested antithyroid medications; PTU and apigenin, significantly reduced the elevated levels of thyroid hormones, the main cause for dyslipidemia occurrence, this consequently normalized the lipid profile. The ability of PTU to normalize lipid profile during treatment of hyperthyroidism was observed in previous investigations [59, 60]. Apigenin beneficial effects on hyperthyroidism associated dyslipidemia was not tested before. However, its capability to correct dyslipidemias associated with other disorders was previously

proven [61, 62]. This was attributed to upregulating fatty acid oxidation, tricarboxylic acid cycle, oxidative phosphorylation, electron transport chain and cholesterol homeostasis gene expression together with downregulating expression of lipolytic and lipogenic genes and decreasing activities of triglyceride and cholesterol ester synthesis enzymes in the liver [60].

### 3.5. Estimation of Hyperthyroidism-Associated LVH

Hyperthyroidism is considered an independent risk factor for cardiomegaly and LVH [63]. In the current investigation, hyperthyroidism was associated with significant increase in LVW/BW%, cardiomyocyte size (assessed by morphometric analysis of cardiomyocyte width in H&E stained left

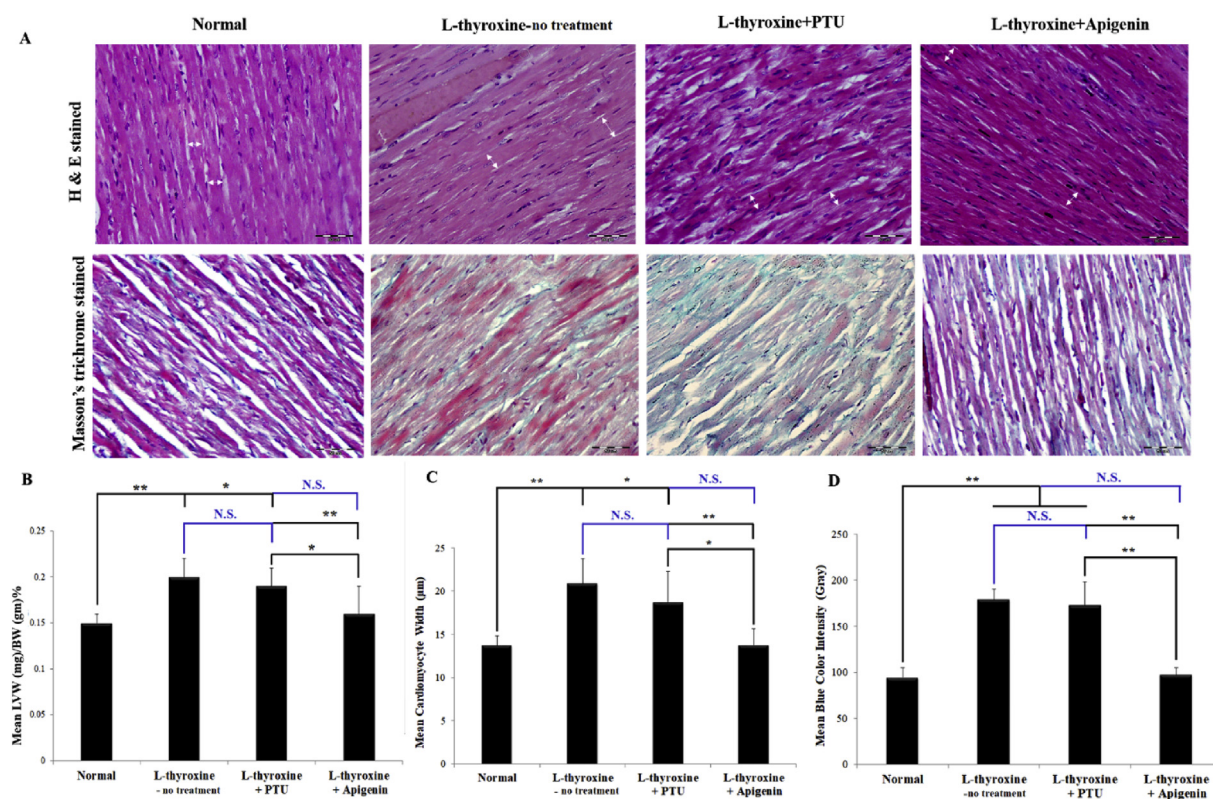
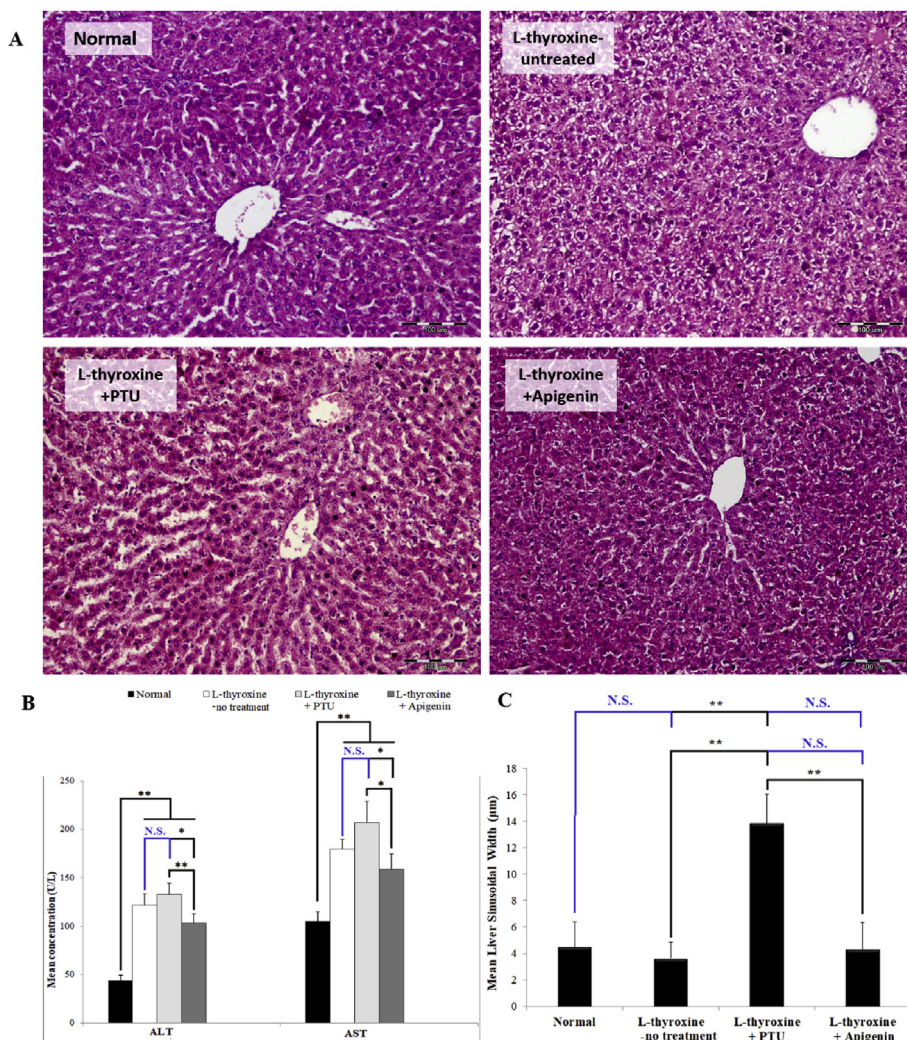


Fig. 6. Effect of different therapies on left ventricular hypertrophy. A; Upper row shows H&E stained left ventricular tissue sections showing cardiomyocytes with longitudinal circular midwall muscle bundles obtained from different groups under magnification  $\times 400$  (double headed white arrows show examples of some selected sites for measuring myocyte width), lower row shows Masson's trichrome left ventricular-stained tissue sections under magnification  $\times 400$ . B; assessment of the percentage of left ventricular weight (LVW) in mg relative to total body weight (BW) in g in different experimental groups. C; Quantification of the mean myocyte width measured in 50 cells per each H&E stained sections of left ventricle samples using ImageJ software. D; Quantification of the mean blue color intensity (representing the amount of fibrous tissue) in Masson's trichrome stained left ventricles sections. ANOVA test was used to compare between the different groups with Post Hoc Test (Tukey). \*: Statistically significant at  $p \leq 0.05$ , \*\*: Statistically significant at  $p \leq 0.001$ , N.S: Statistically non-significant ( $p > 0.05$ ),  $n = 8$ ; all results are presented as mean  $\pm$  SD.



**Fig. 7.** Effect of different drugs on liver histology and enzymes. **A;** H&E-stained liver tissue sections obtained from different groups under magnification power  $\times 200$ . **B;** biochemical assessment of liver enzymes in sera obtained from rats of different groups (ALT: alanine aminotransferase, AST: aspartate aminotransferase). **C;** quantitative estimation of mean hepatic sinusoidal width measured in H & E stained liver tissue sections using imageJ software. ANOVA test was used to compare between the different groups with Post Hoc Test (Tukey). \*: Statistically significant at  $p \leq 0.05$ , \*\*: Statistically significant at  $p \leq 0.001$ , N.S: Statistically non-significant ( $p > 0.05$ ),  $n = 8$ ; all results are presented as mean  $\pm$  SD.

ventricular sections) and amount of fibrous tissue (quantified by analyzing the intensity of blue color (fibrous tissue) in Masson's trichrome stained left ventricles tissue sections) compared to normal rats (Fig. 6). LVH associated with hyperthyroidism is due to increased supersensitivity of the heart to minimal changes in serum thyroid hormone levels that causes cardiac genomic and nongenomic actions resulting in many hemodynamic and cardiovascular manifestations of this disease [64]. In addition, thyroid hormones elevation stimulates cardiac protein

synthesis leading to a concentric cardiac hypertrophy [65]. It should be noted that serum T3, and not T4, is the primary thyroidal hormone which act on the heart and that cardiac tissue totally lack intracellular activity of IDI [66]. In the present study, the prominent increase in left ventricular interstitial fibrosis was observed accompanying the state of hyperthyroidism. A study done by Kotajima et al. confirmed a significant positive correlation between thyroid hormones and serum level of transforming growth factor beta 1 (TGF- $\beta$ 1), which is the strongest

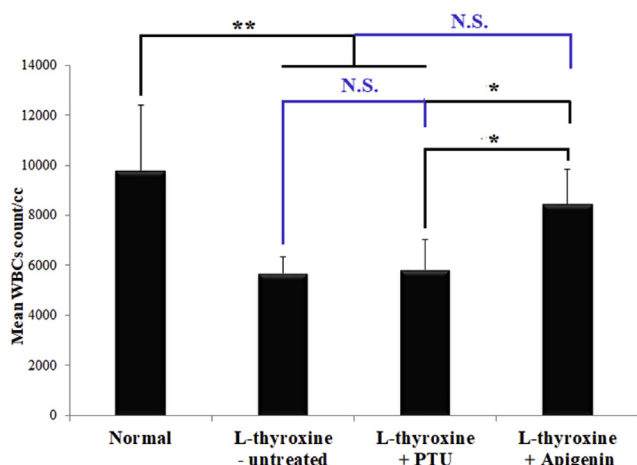


Fig. 8. Effect of different therapies on white blood cell count in rats with L-thyroxine-induced hyperthyroidism ANOVA test was used to compare between the different groups with Post Hoc Test (Tukey). \*: Statistically significant at  $p \leq 0.05$ , \*\*: Statistically significant at  $p \leq 0.001$ , N.S: Statistically non-significant ( $p > 0.05$ ),  $n = 8$ ; all results are presented as mean  $\pm$  SD.

known profibrogenic mediator [67]. Cardiac hypertrophy is greatly affected by the production of the extracellular matrix by fibroblasts mediated by TGF- $\beta$ 1 [68].

In this investigation, apigenin, but not PTU therapy, significantly reduced LVW/BW%, mean cardiomyocyte width and mean amount of fibrous tissue in left ventricles compared to untreated group. Moreover, apigenin-treated group had shown no significant difference in all assessed parameters compared to normal group, Fig. 6. Since there was no significant difference in mean serum T3 level between apigenin and PTU-treated groups, other molecular mechanisms may contribute to the dissimilar results of both therapies on hyperthyroidism-induced LVH that need extra investigations. Consistent with our results regarding PTU therapy, common cardiovascular abnormalities accompanying hyperthyroidism persisted despite effective PTU antithyroid therapy in L-thyroxine induced hyperthyroidism in FVB/N male mice [69], in rats [70] and in patients with overt hyperthyroidism [71]. Concerning the effect of PTU on cardiac fibrosis, there is a common agreement on the association of hypothyroidism and cardiac fibrosis [67, 72]. In the current study, PTU significantly reduced TSH below normal level and thus it is expected to observe

significant intracellular matrix deposition in left ventricular tissue as evident in Masson's trichrome stained tissue sections.

Although the effect of apigenin in hyperthyroidism associated cardiovascular abnormalities was not tested before. Many studies in other disease conditions proved the favorable effects of apigenin on cardiovascular illnesses [73-75]. Apigenin attenuated induced myocardial injury in diabetic rats [73]. It also alleviated cardiac remodeling and reduced cardiac interstitial fibrosis in streptozotocin-induced diabetic cardiomyopathy [75]. Furthermore, apigenin improved hypertensive cardiac dysfunction and myocardial glucolipid metabolism in a rat cardiac hypertrophy model induced by renovascular hypertension [74].

### 3.6. Comparing Toxicities Associated With Antithyroid Therapies

#### 3.6.1. Evaluation of hepatotoxicity biochemically and histologically

A significant elevation in serum liver enzymes compared to normal rats' level was observed in the present work (Fig. 7). H&E stained liver tissue sections obtained from normal rats showed normal liver architecture with no signs of hepatocyte necrosis, hemorrhage or inflammation. On the other hand, liver tissues obtained from untreated rats with induced hyperthyroidism showed signs of liver damage such as some degree of fatty infiltration, cytoplasmic vacuolization and nuclear irregularity. In addition, hepatocytes cell swelling as a result of defects in cell permeability or mitochondrial dysfunction was observed. The mean sinusoidal space width was not significantly different and is even less than that of normal liver tissues and this could be due to the noticeable hepatocytes swelling. Hyperthyroidism-induced hepatotoxicity is due to increased metabolism with subsequent oxidative damage to many organs including the hepatic systems [76]. This induced hepatic dysfunction is provoked by excess T3 which induces hepatocyte apoptosis resulting in liver dysfunction via activation of the mitochondrial-dependent pathway [77].

Daily PTU therapy to rats with induced hyperthyroidism for 21 days resulted in a non-significant reduction in ALT or AST levels as compared to

positive control group. Tissue sections obtained from rats treated with PTU showed severe liver damage manifested by massive necrosis and inflammation. A significant increase in the mean sinusoidal space width was detected when compared to that of normal liver sections. PTU-induced hepatotoxicity is a result of drug induced idiosyncratic reaction that include allergic reactions and immune-mediated liver function impairment. Also, PTU is metabolized into a bioactive metabolite that is hepatotoxic [78]. Another proposed mechanism is the induced mitochondrial dysfunction by PTU [79].

Apigenin therapy for 3 successive weeks produced a significant decrease in the serum ALT and AST concentrations in comparison with positive control group and PTU-treated group, Fig. 7. Liver sections obtained from apigenin-treated rats treated showed nearly normal liver architecture with some vacuolated hepatocytes. The mean sinusoidal space width was comparable to that in normal liver tissue sections, Fig. 7. Apigenin had hepatoprotective effects in induced liver damage by modulating metabolic and transcriptional profiles in the liver [61], by regulating hepatic oxidative stress [80], and increased the levels of hepatic nuclear factor erythroid 2-related factor 2-mediated antioxidant enzymes [81].

### 3.6.2. Assessing the potential of developing agranulocytosis

Agranulocytosis development can be predicted by counting WBCs. Both positive control group and PTU-treated groups had significantly less WBC count than that of normal rats, Fig. 8. Hyperthyroidism status was found to cause decreases in total WBC count, neutropenia, thrombocytopenia as a result of hyperplasia in all myeloid cell lineages. In addition, T3 is as a precursor for normal B cell formation in bone marrow through pro-B cell proliferation stimulation [82]. On the other hand, the thioamide group PTU is the cause of its various hematologic side effects ranging from mild leukopenia to agranulocytosis and aplastic anemia [83]. Apigenin therapy significantly restored WBCs count compared to both positive control group and PTU-treated group, Fig. 8. Likewise, apigenin did not alter WBC counts when tested for its antineoplastic potential in renal cell carcinoma [84], and restored

myeloid series in SCID mice bearing K562 disseminated leukemia model [85].

## 4. Conclusion

From the aforementioned data, apigenin seemed to have the highest *in silico* and *in vitro* antithyroid activity among all identified *Medicago sativa* L. sprouts phytoconstituents. *In vivo* studies revealed that apigenin antithyroid mechanism is via inhibition of TPO and more prominently, IDI-1. Moreover, apigenin therapy was superior to PTU in achieving nearly euthyroid state (without incidence of hypothyroidism or thyroid gland hypertrophy or hyperplasia). In addition, apigenin, but not PTU, corrected hyperthyroidism-induced LVH without noteworthy liver toxicity or reduction of WBCs count. Thus, apigenin may represent a possible safer alternative to conventional antithyroid drugs.

## Associated content

<sup>1</sup>H NMR, APT, HMQC, HMBC and COSY spectral analyses, supplementary (Tables T1-T4) and (Fig. S1-S35).

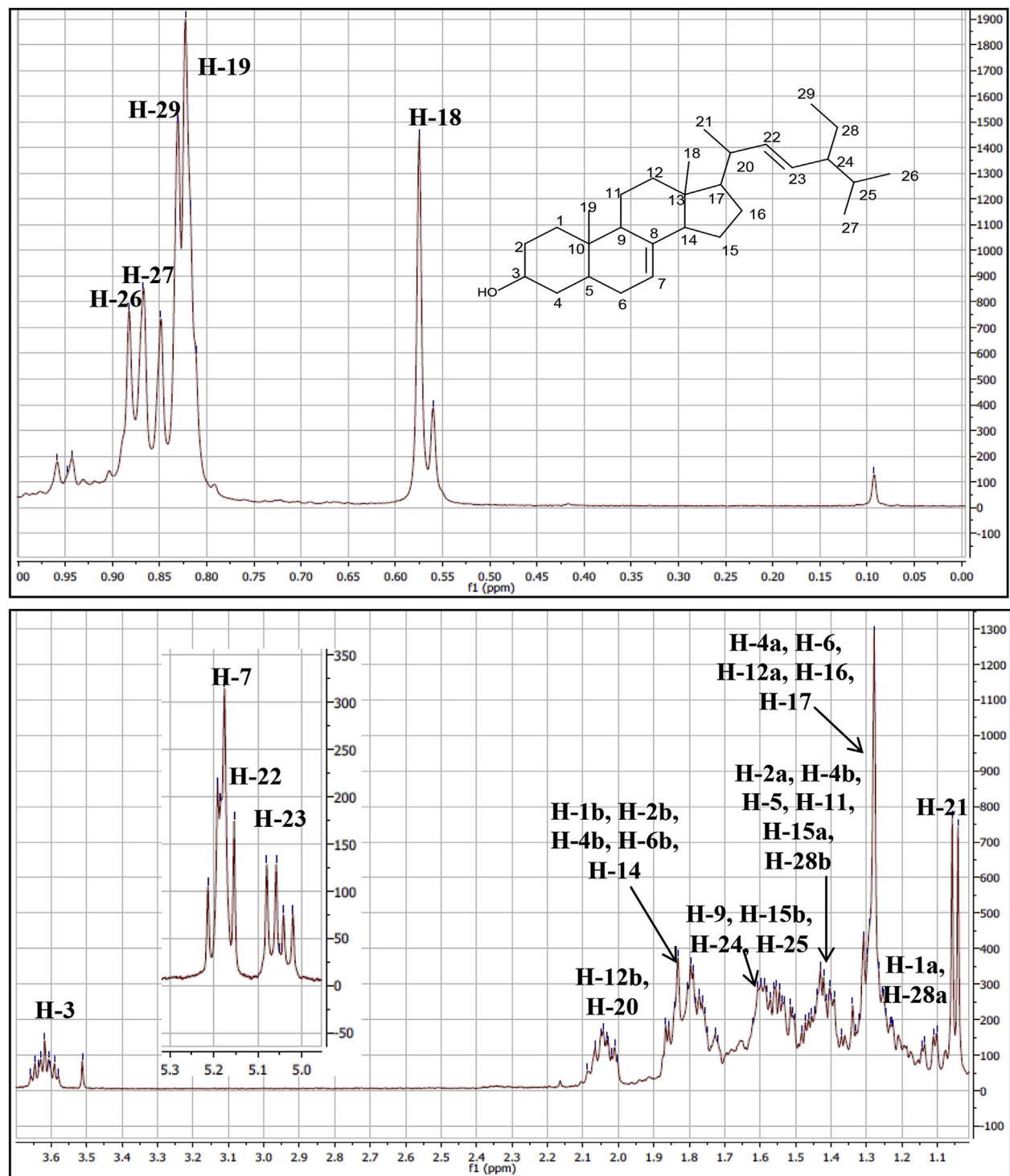
## Declaration of interest

This research did not receive any specific grant from funding agencies in the public, commercial, or not-for-profit sectors. The authors report no financial or personal conflict of interest.

## Acknowledgment

The authors would like to acknowledge Dr. R.A. Abd el Moneim (assistant professor in histology and cell biology, Faculty of Medicine, Alexandria University, Alexandria, Egypt) for her aid in the interpretation of histopathological results. Further, authors acknowledge R.M. Farouk, Y.A. El-Sayed, R.S. Salem, N.Y. Tehemar, N.A. El-Kharadly, M.M. Emam, A.H. Zayed, A.H. Raslan, Z.A. Ashour, M.R. Omar and A.O. Emara (Faculty of Pharmacy and Drug Manufacturing, Pharos University in Alexandria, Alexandria, Egypt) for their contribution in performing some practical experiments, under authors' supervision, as a part of their graduation project.

## Appendix.

Fig. S1.  $^1\text{H}$  NMR (500 MHz) spectrum of compound 1 in  $\text{CD}_3\text{OD}$ .

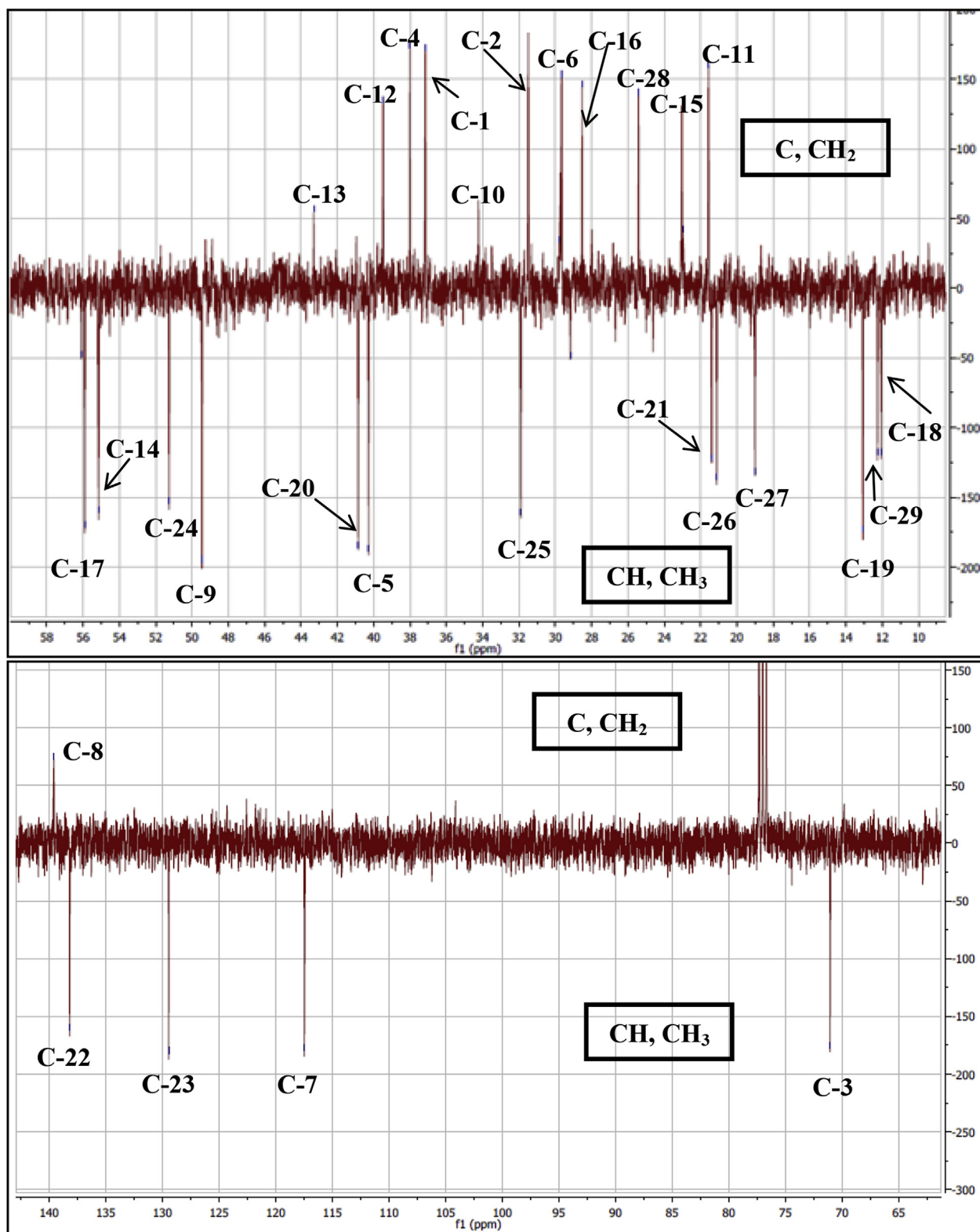


Fig. S2. APT spectrum of compound 1

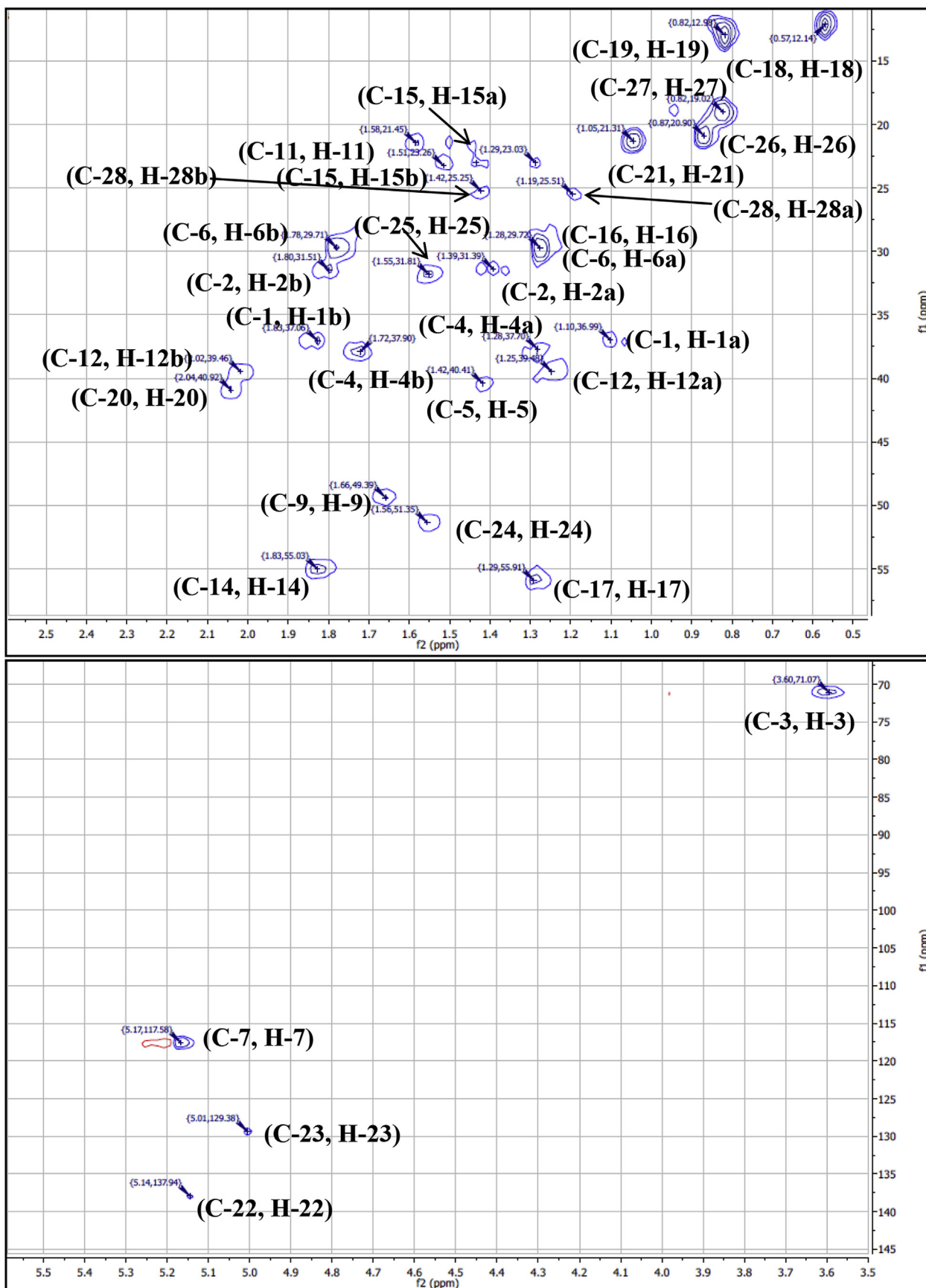


Fig. S3. HMQC spectrum of compound 1.

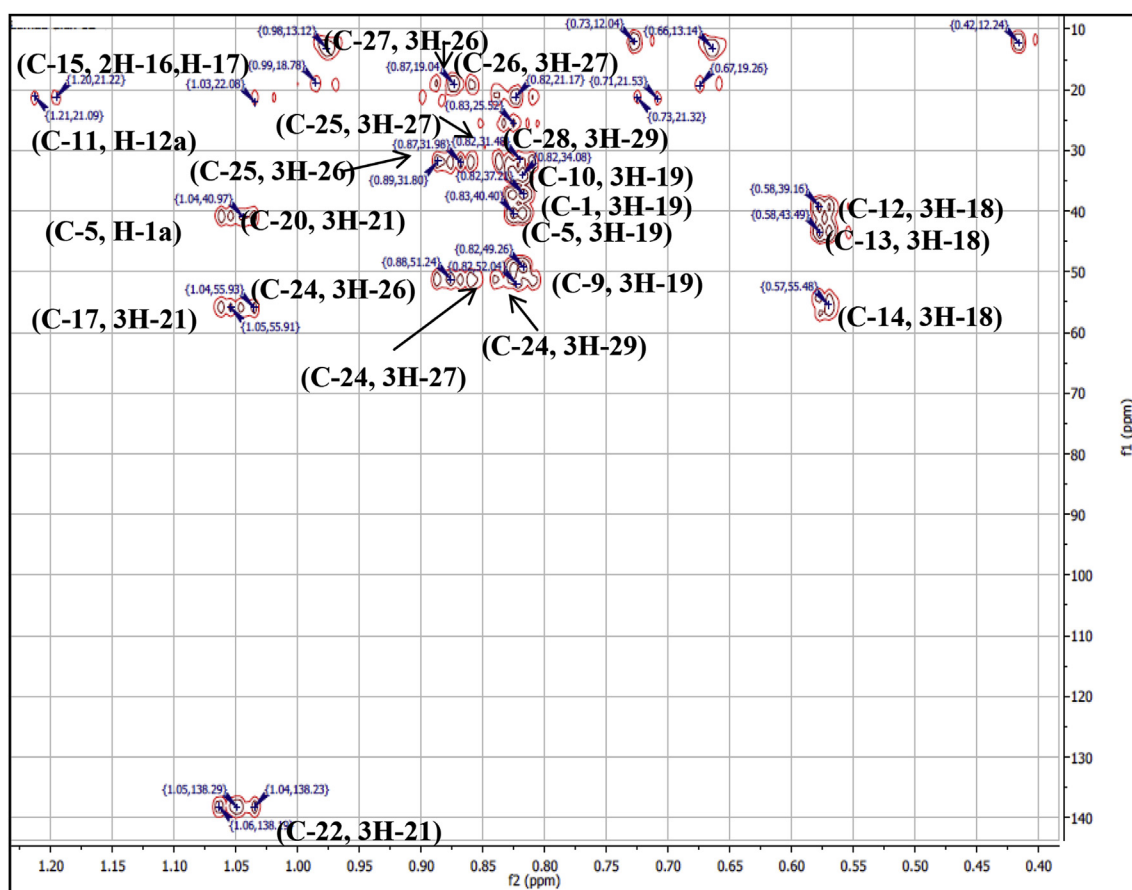


Fig. S4. HMBC spectrum of compound 1.

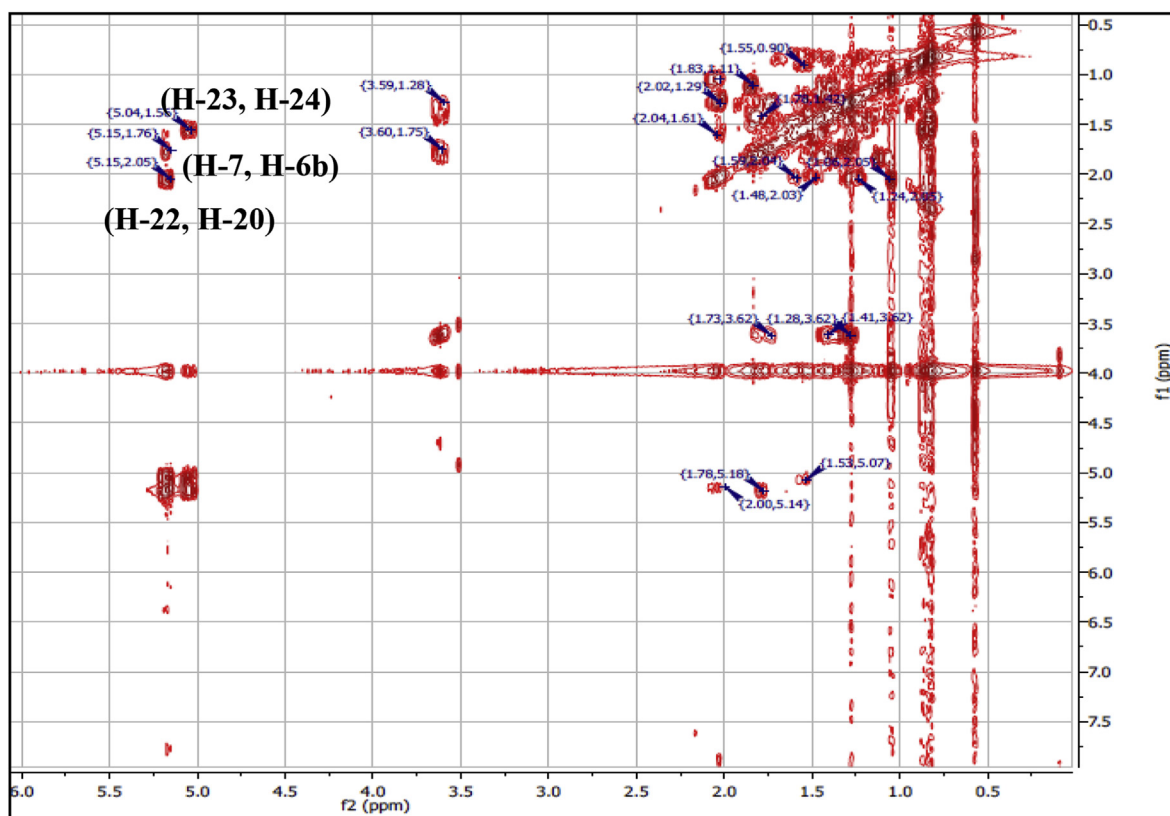


Fig. S5. COSY spectrum of compound 1.

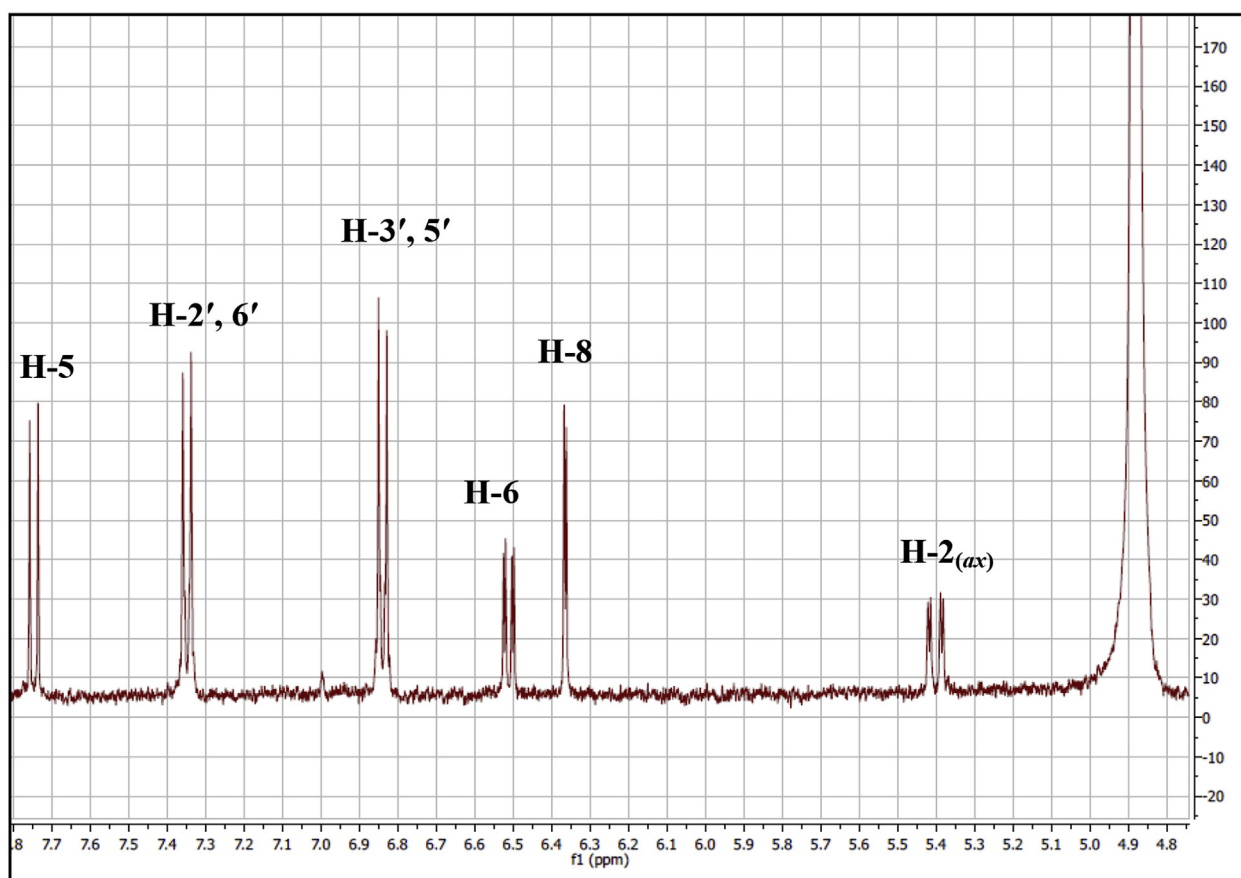
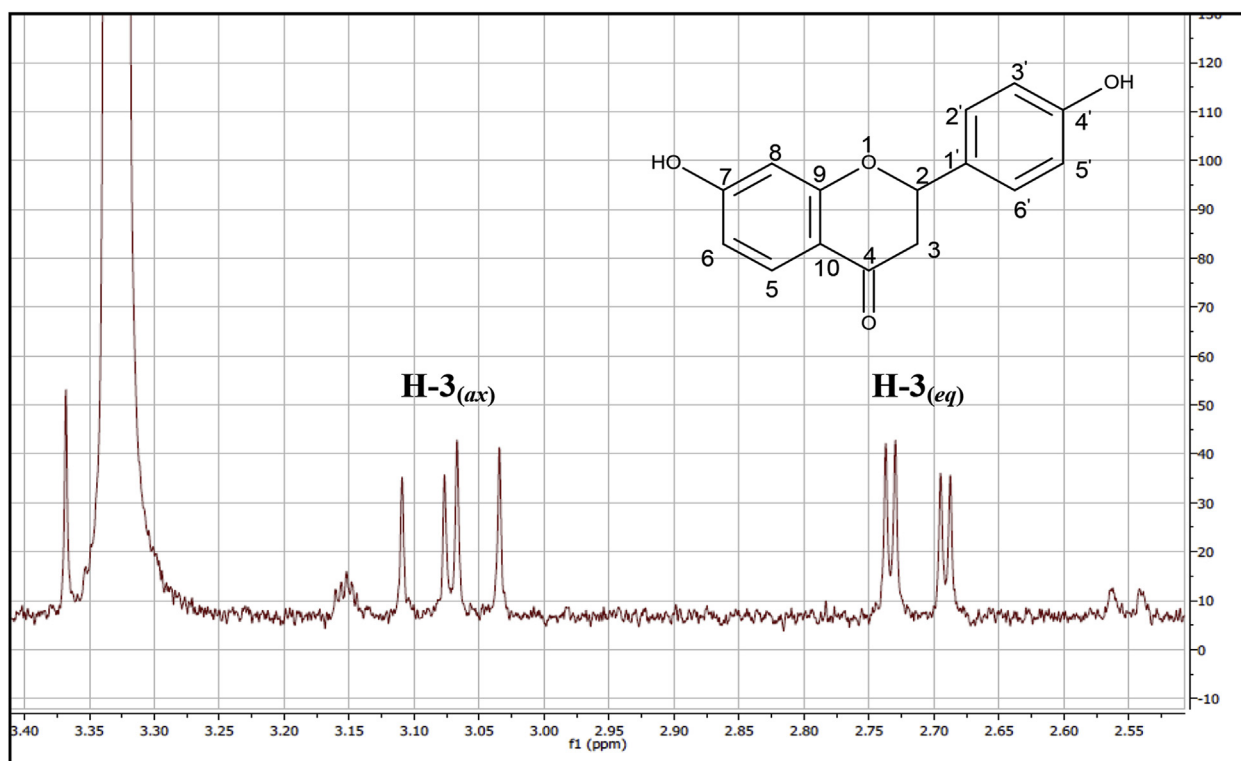


Fig. S6.  $^1\text{H}$  NMR (500 MHz) spectrum of compound 2 in  $\text{MeOH-}d_4$ .

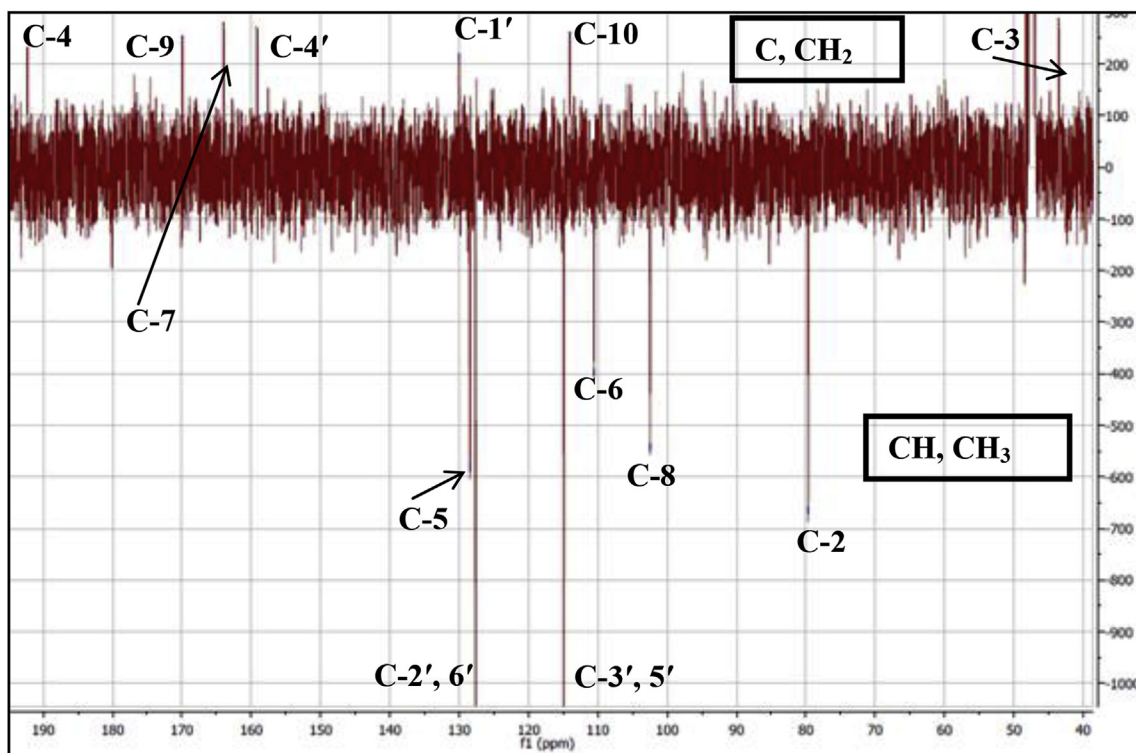


Fig. S7. APT spectrum of compound 2.

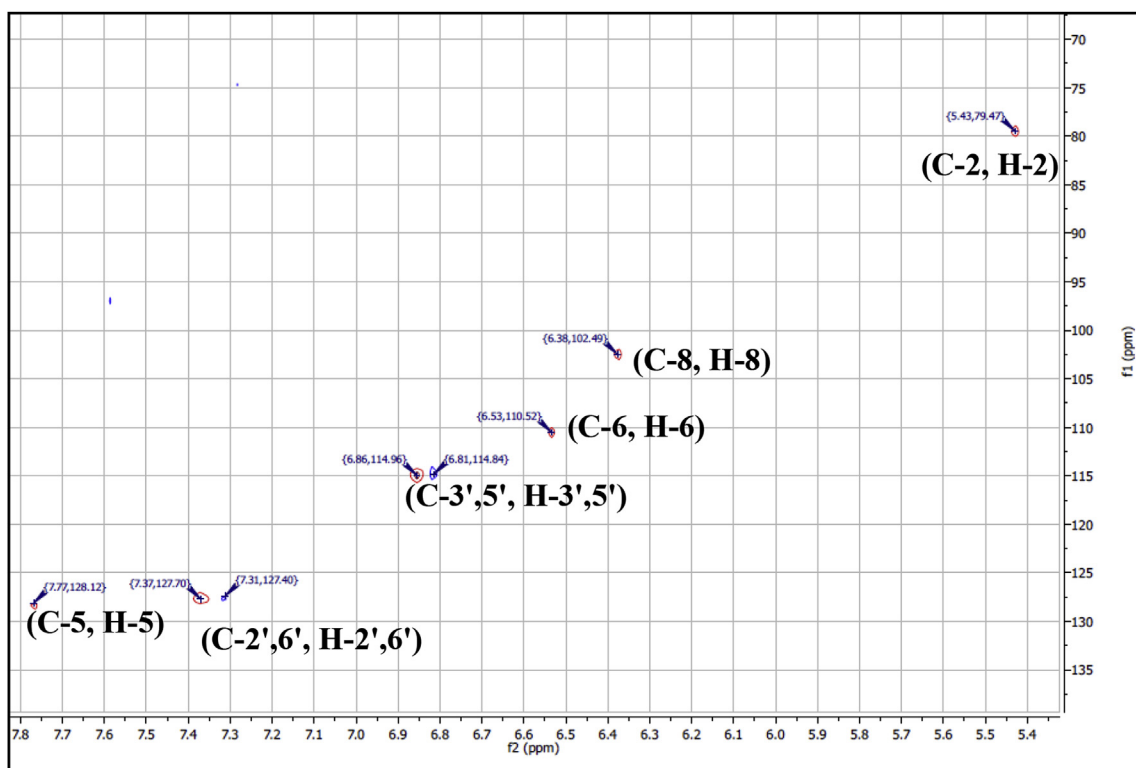


Fig. S8. HMQC spectrum of compound 2.

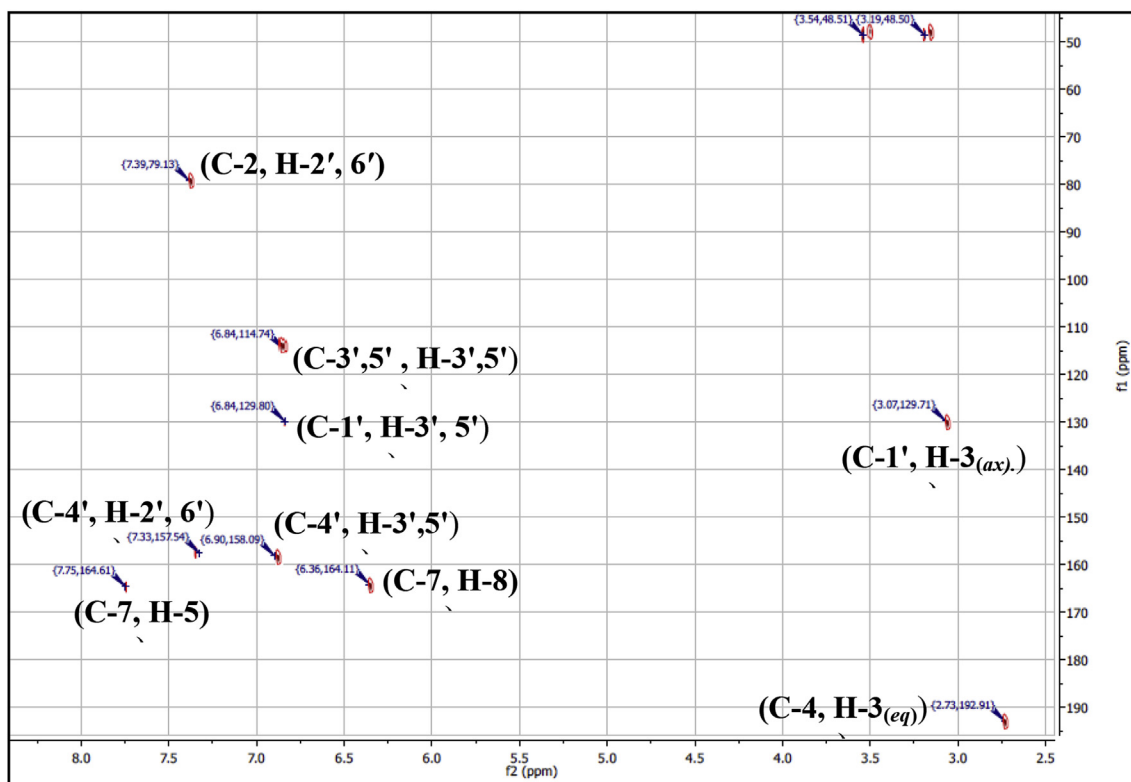


Fig. S9. HMBC spectrum of compound 2.

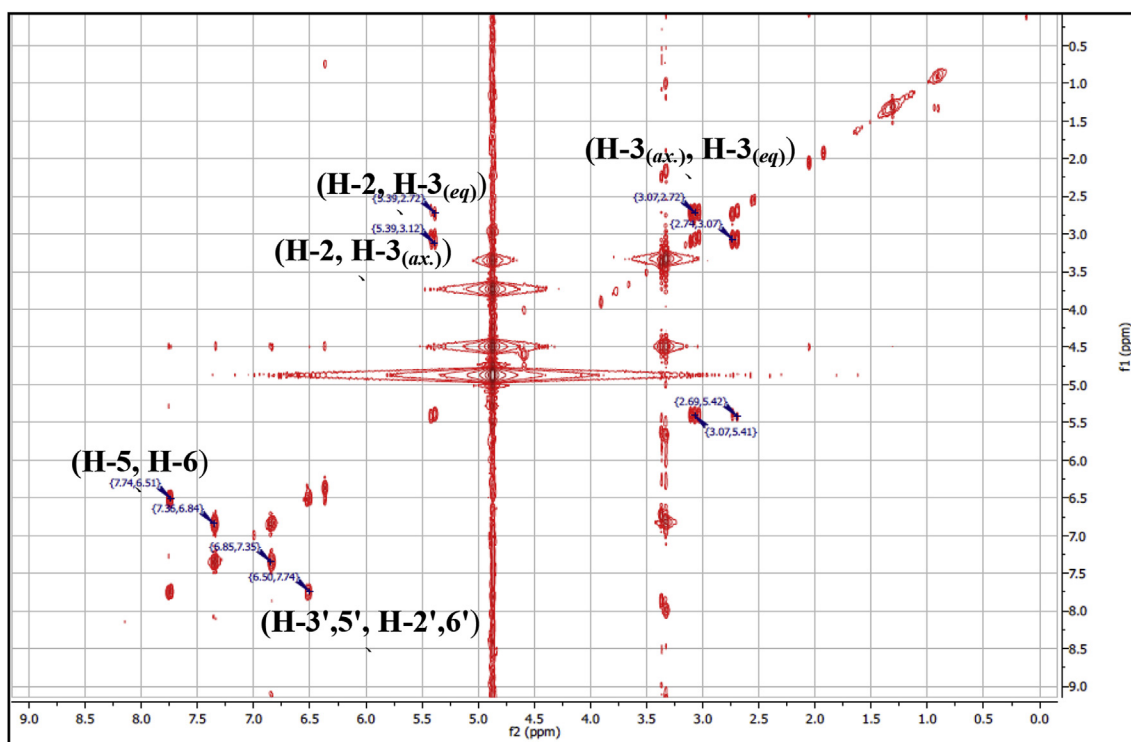


Fig. S10. COSY spectrum of compound 2.

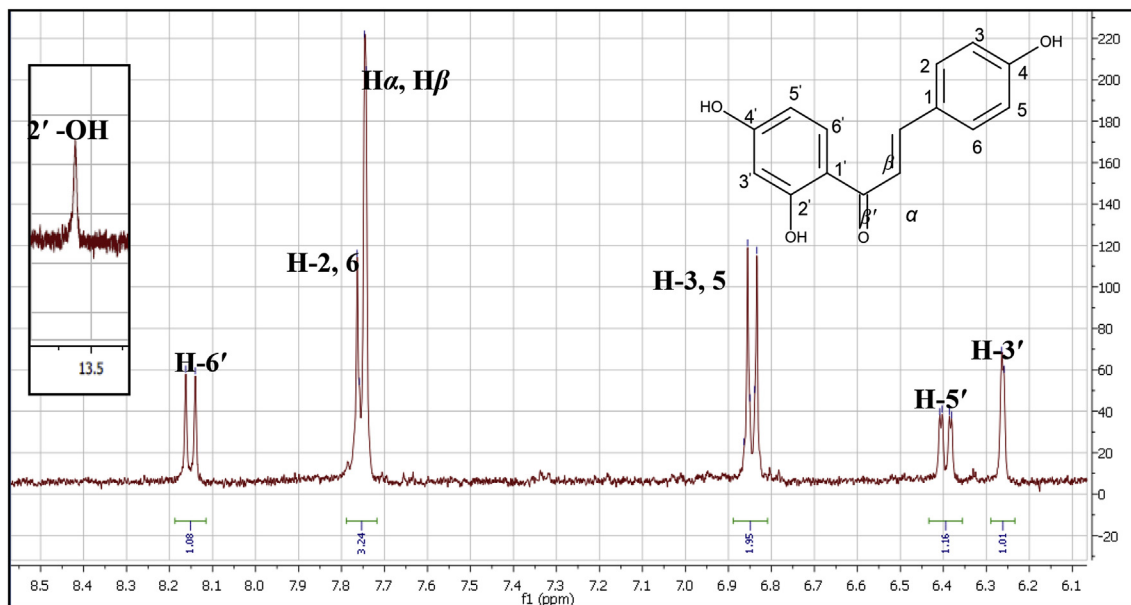


Fig. S11.  $^1\text{H}$  NMR (500 MHz) spectrum of compound 3 in  $\text{DMSO-d}_6$ .

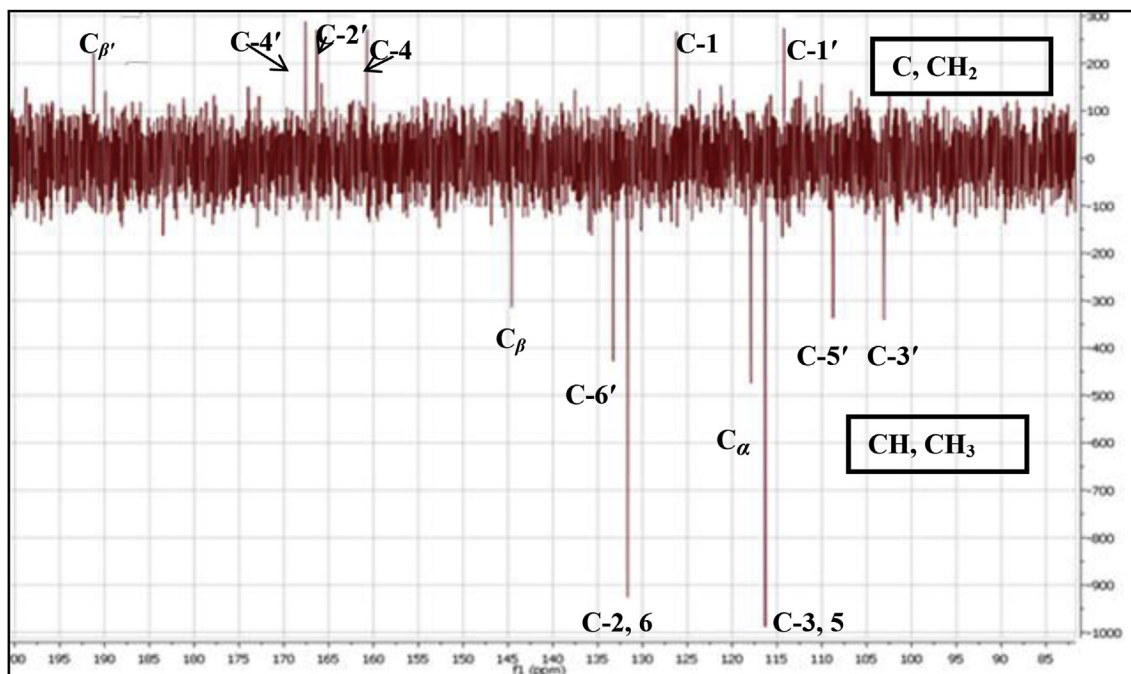


Fig. S12. APT spectrum of compound 3.

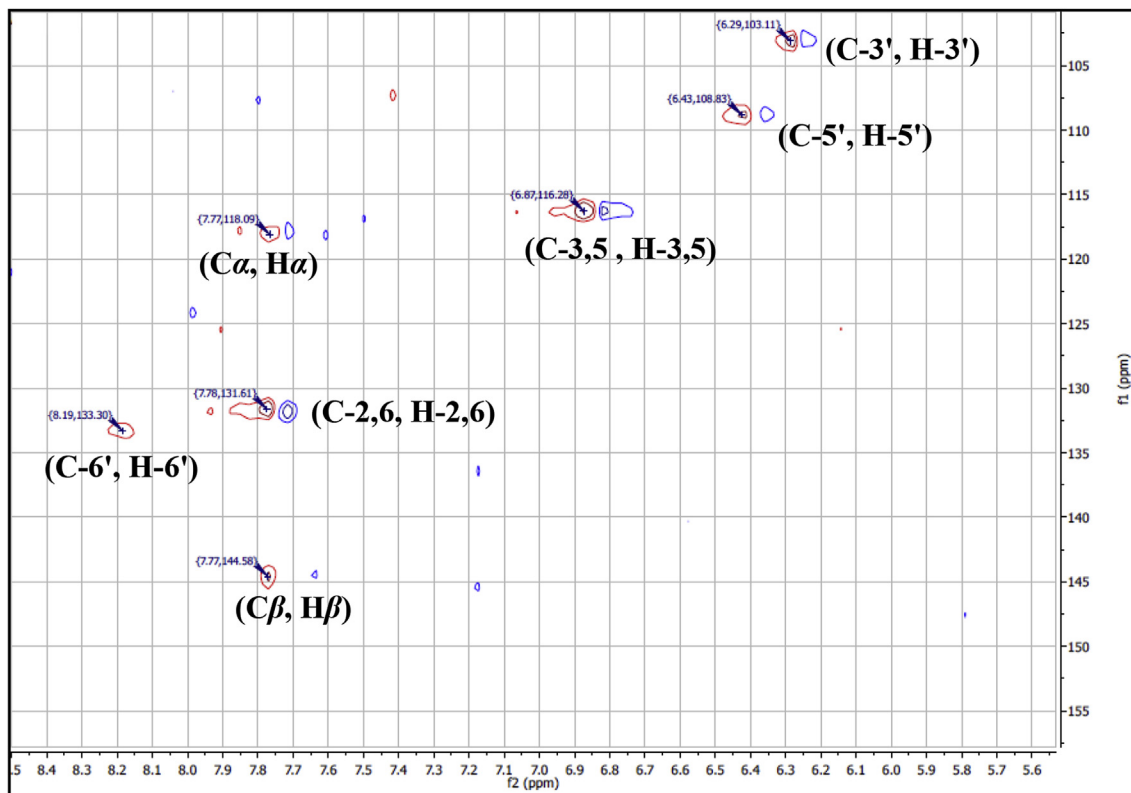


Fig. S13. HMQC spectrum of compound 3.

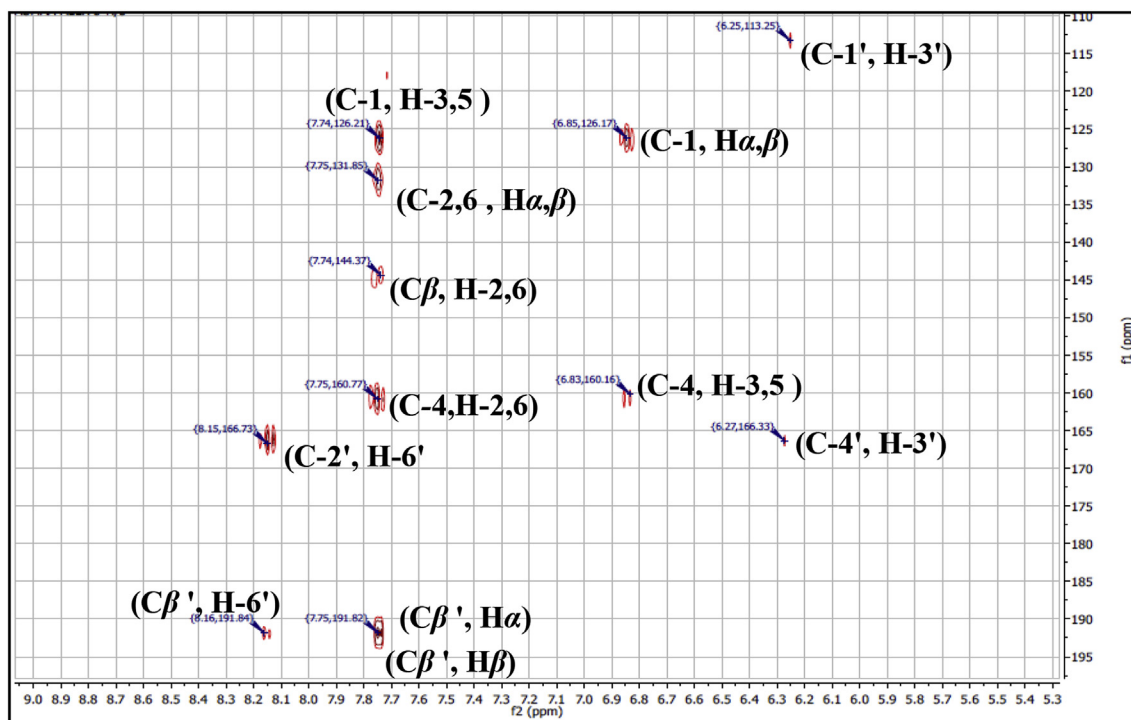


Fig. S14. HMBC spectrum of compound 3.

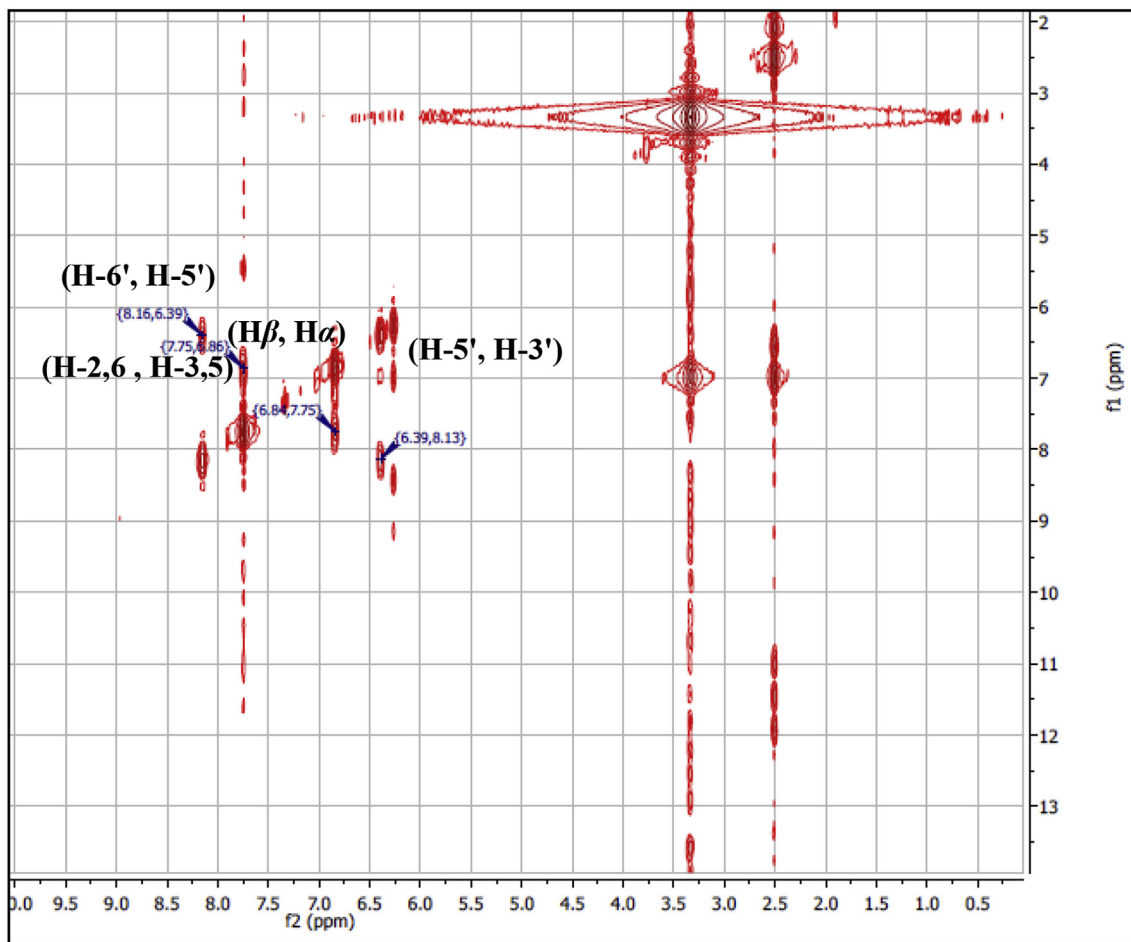


Fig. S15. COSY spectrum of compound 3.

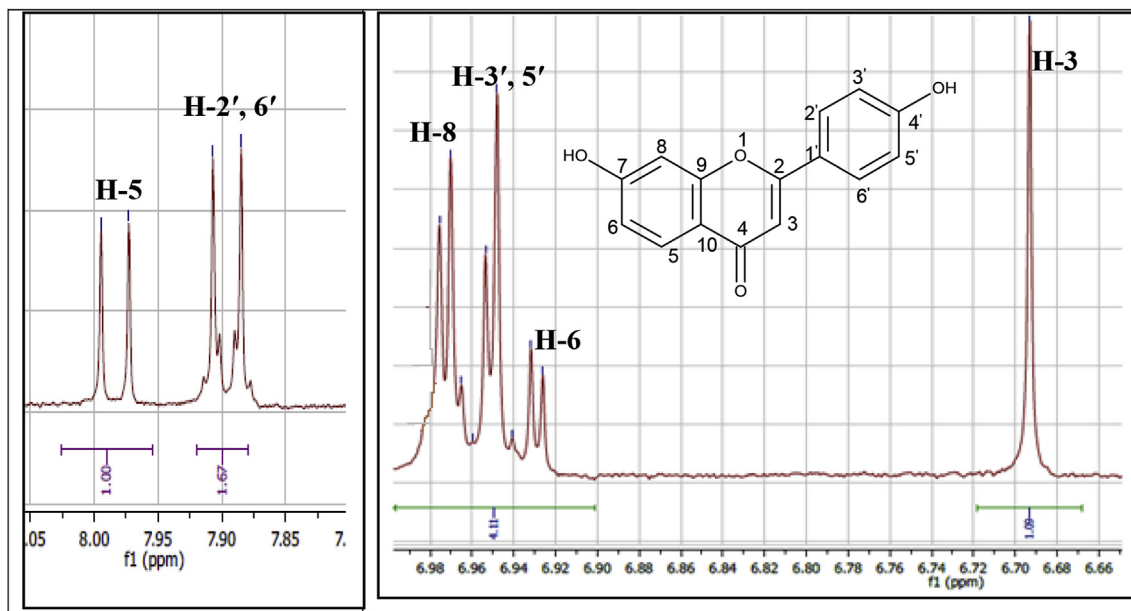


Fig. S16.  $^1\text{H}$  NMR (500 MHz) spectrum of compound 4 in  $\text{MeOH-d}_4$ .

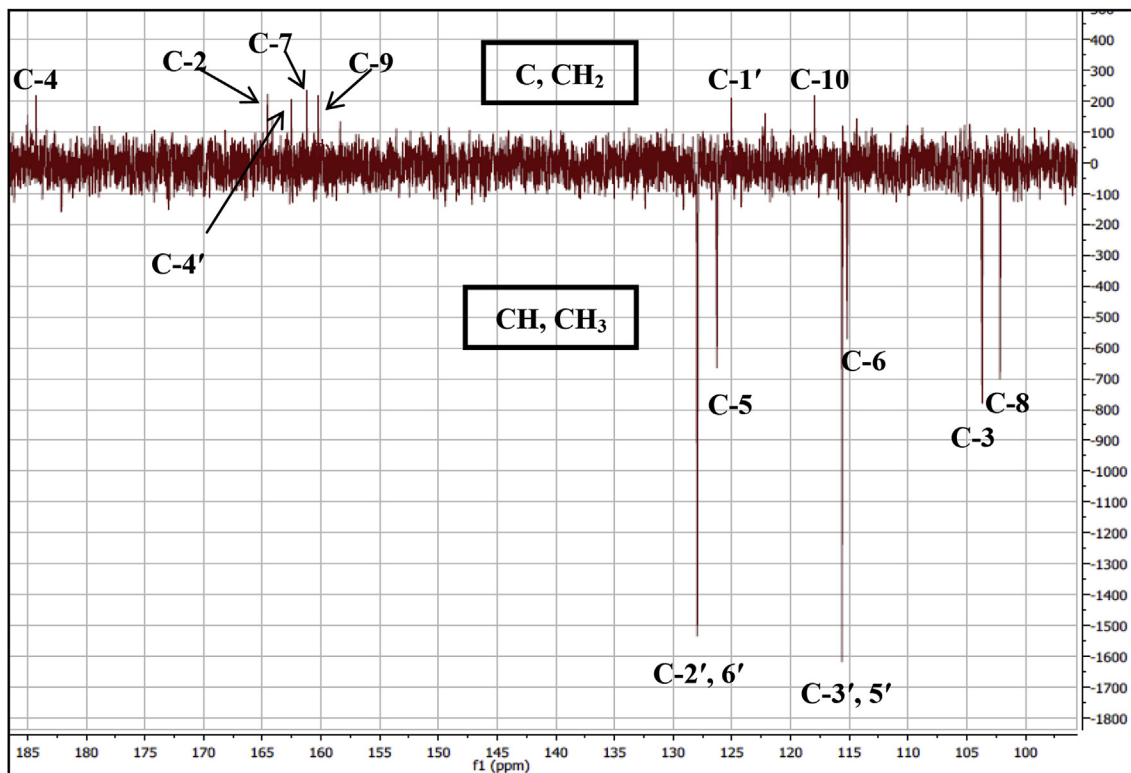


Fig. S17. APT spectrum of compound 4.

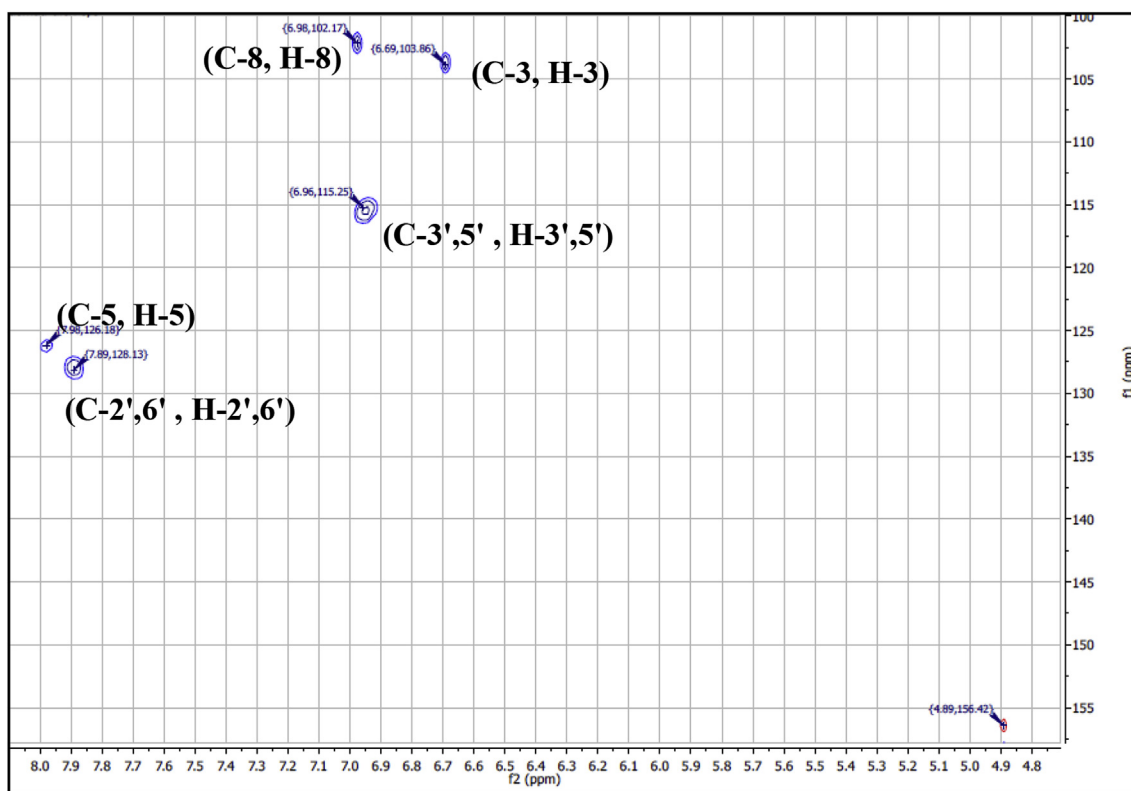


Fig. S18. HMQC spectrum of compound 4.

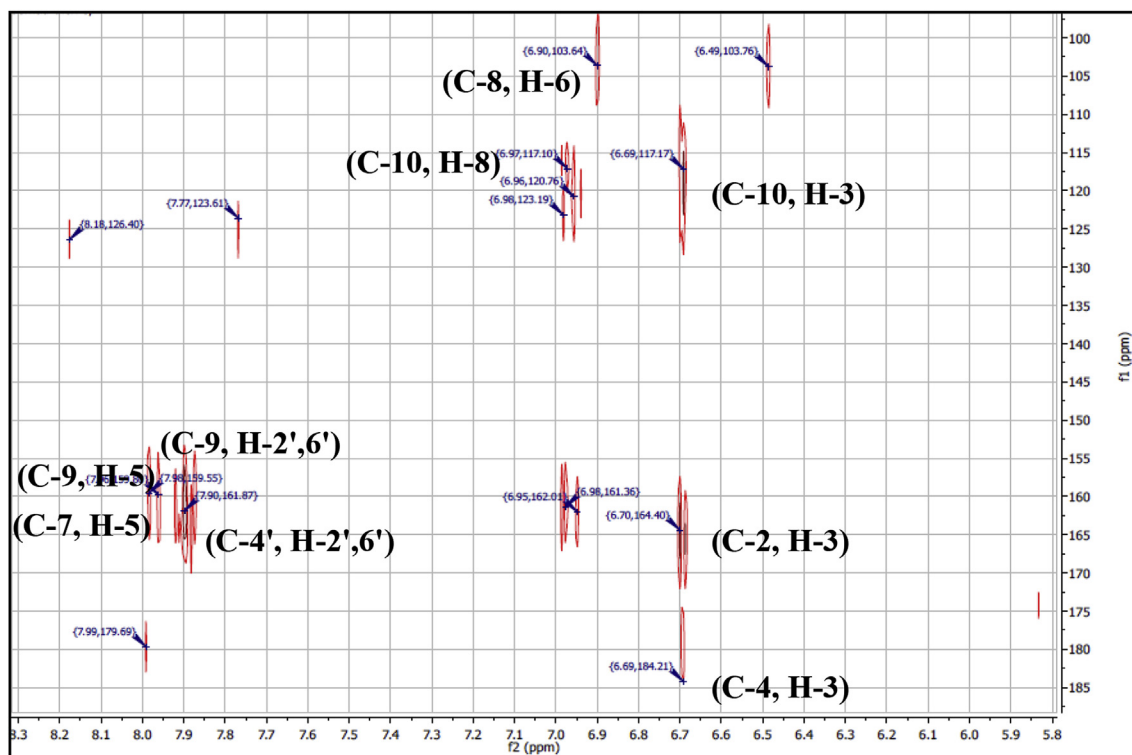


Fig. S19. HMBC spectrum of compound 4.

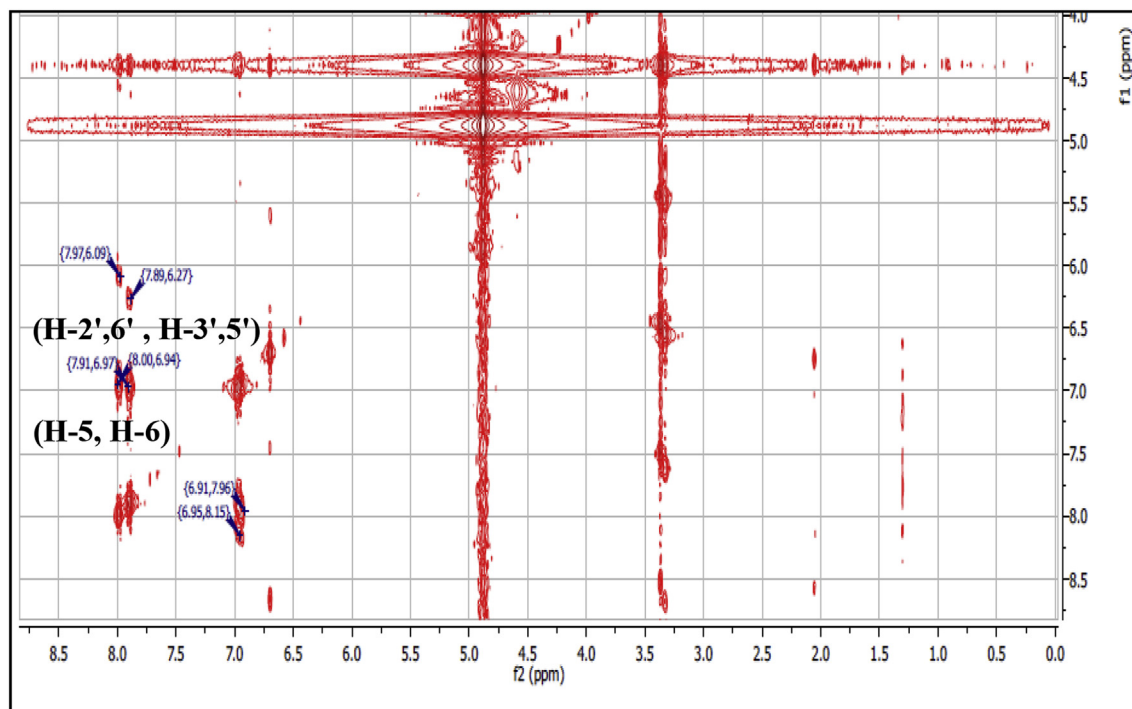


Fig. S20. COSY spectrum of compound 4.

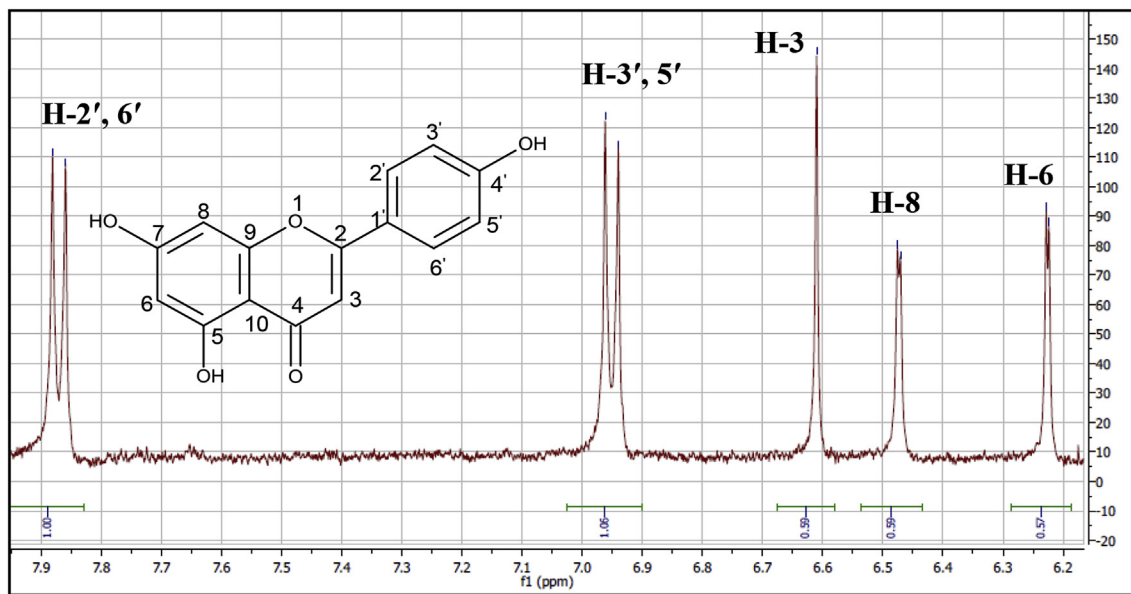


Fig. S21.  $^1\text{H}$  NMR (500 MHz) spectrum of compound 5 in  $\text{MeOH-d}_4$ .

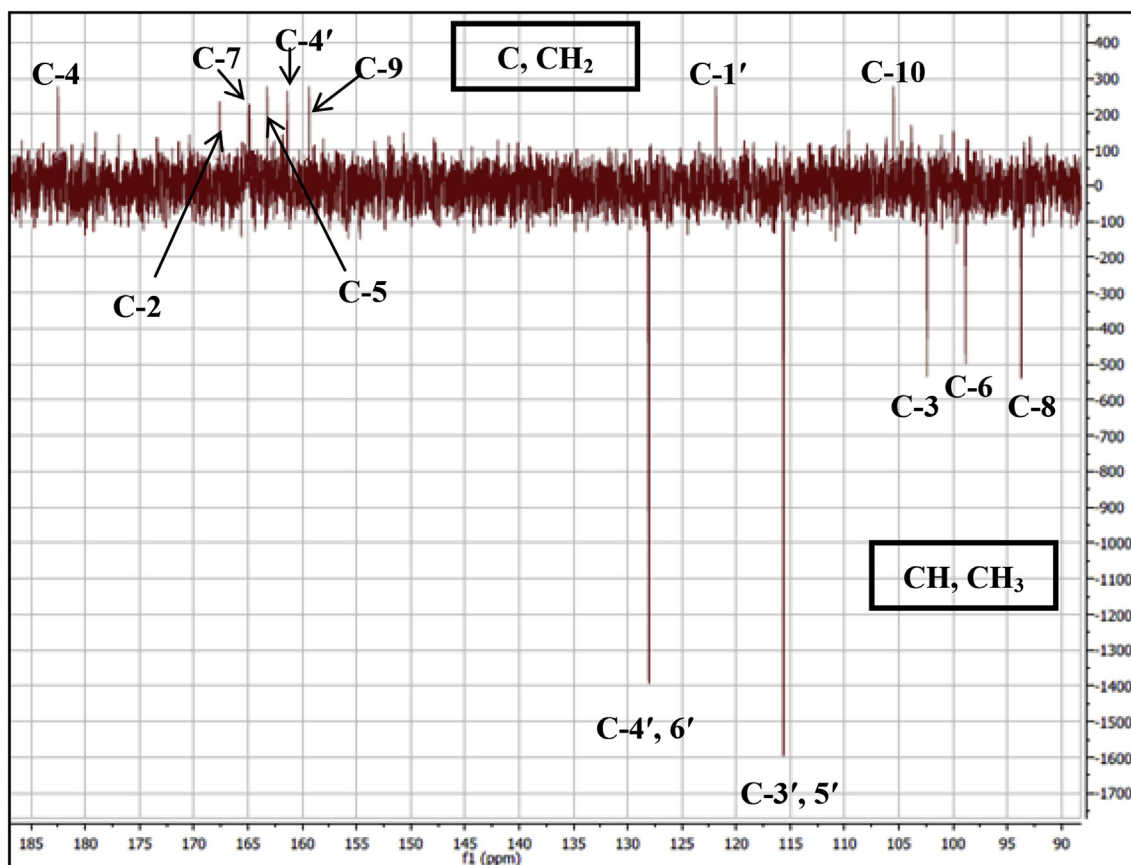


Fig. S22. APT spectrum of compound 5.

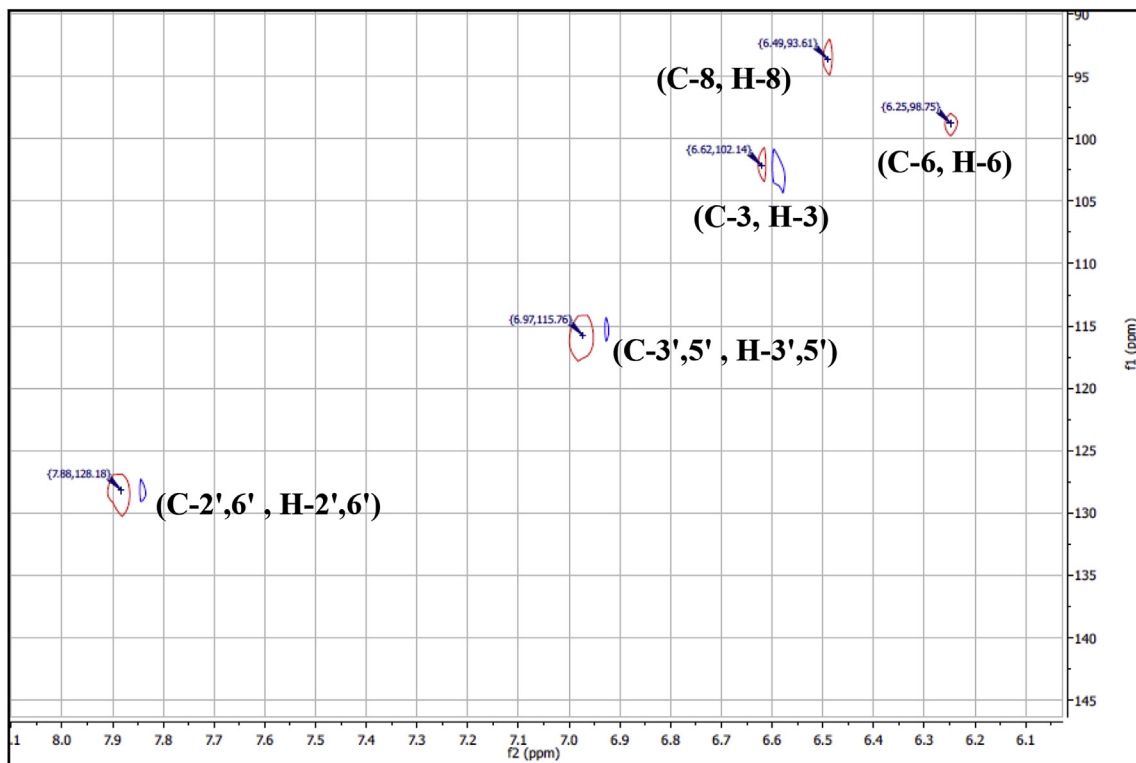


Fig. S23. HMQC spectrum of compound 5.

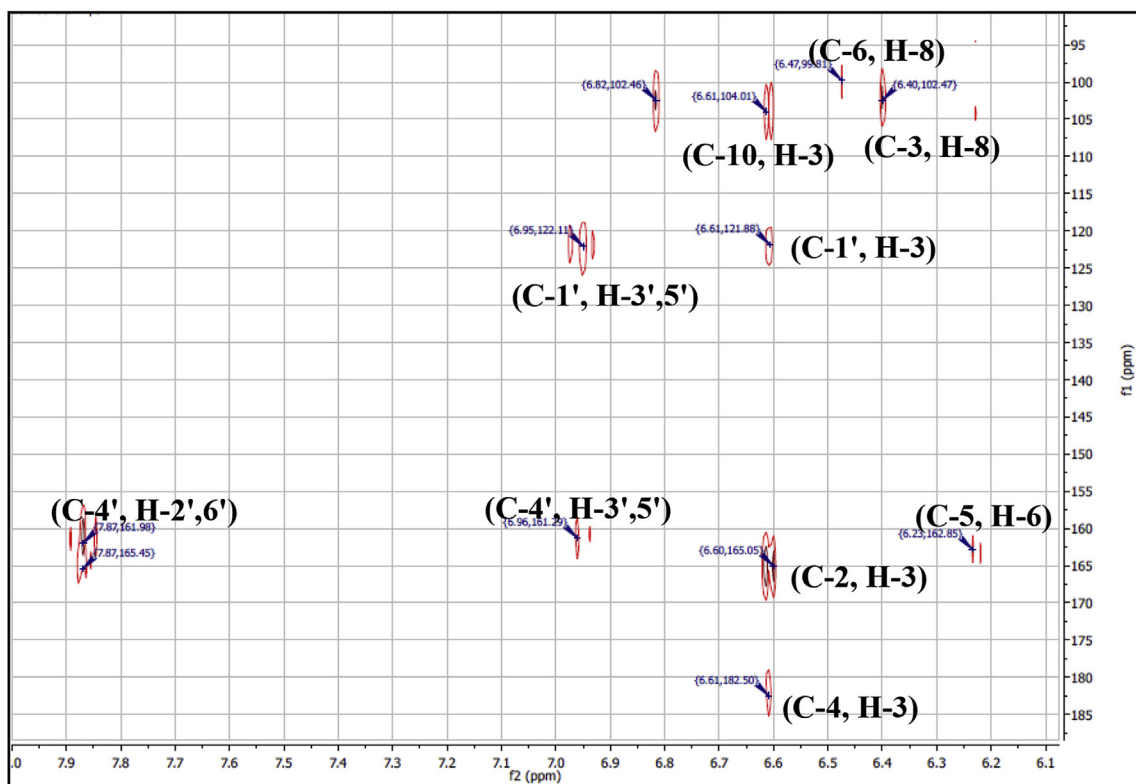


Fig. S24. HMBC spectrum of compound 5.

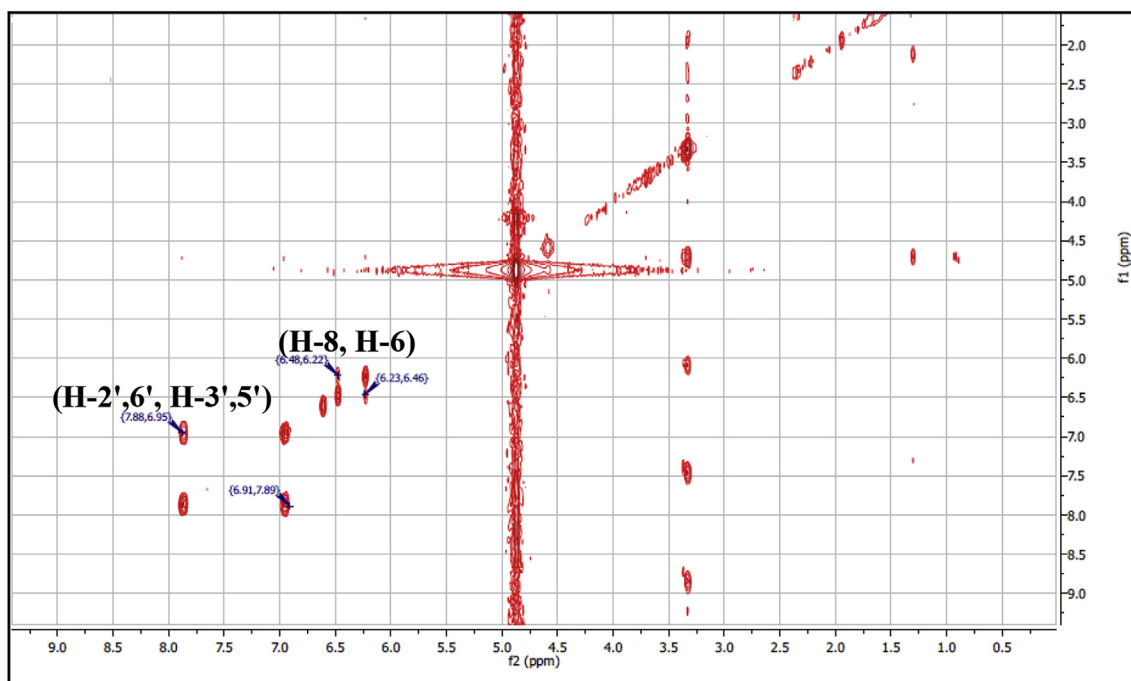


Fig. S25. COSY spectrum of compound 5.

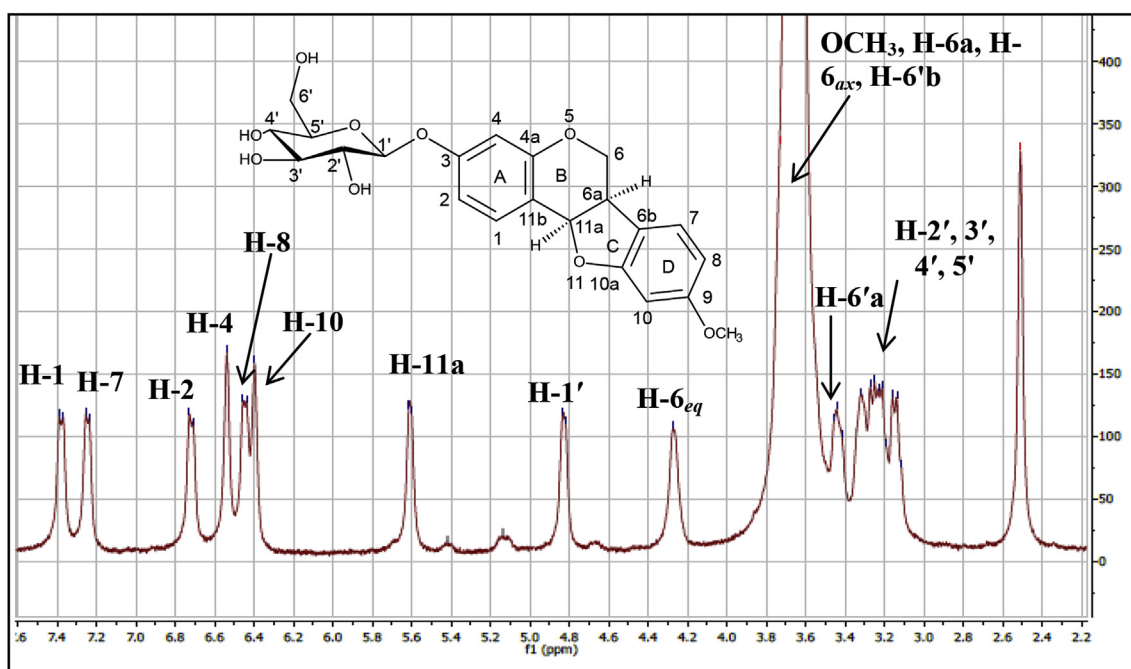


Fig. S26.  $^1\text{H}$  NMR (500 MHz) spectrum of compound 6 in  $\text{DMSO-d}_6$ .

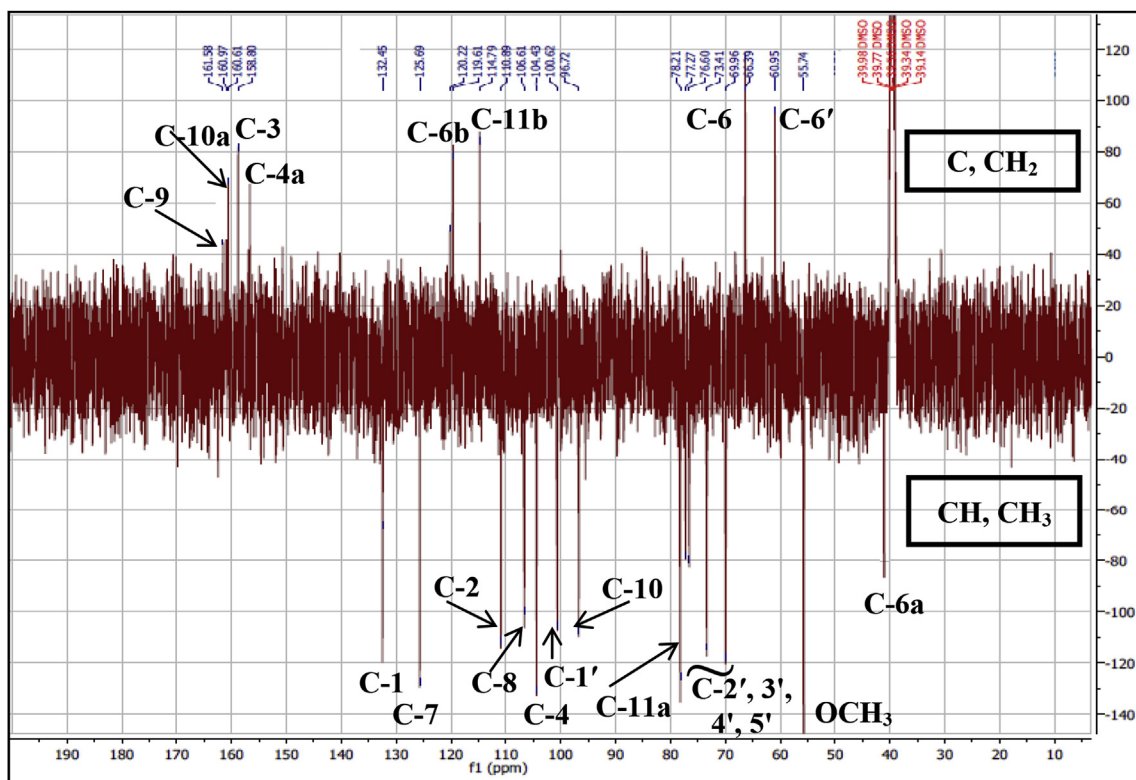


Fig. S27. APT spectrum of compound 6.

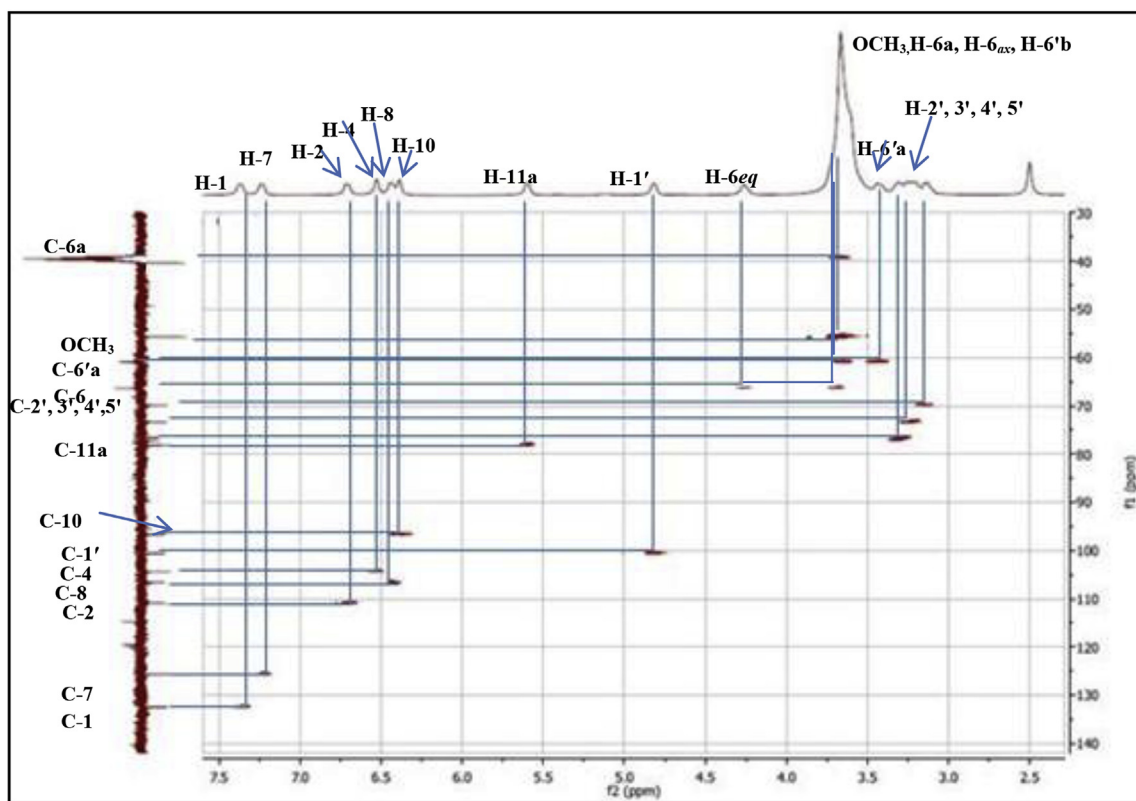


Fig. S28. HMQC spectrum of compound 6.

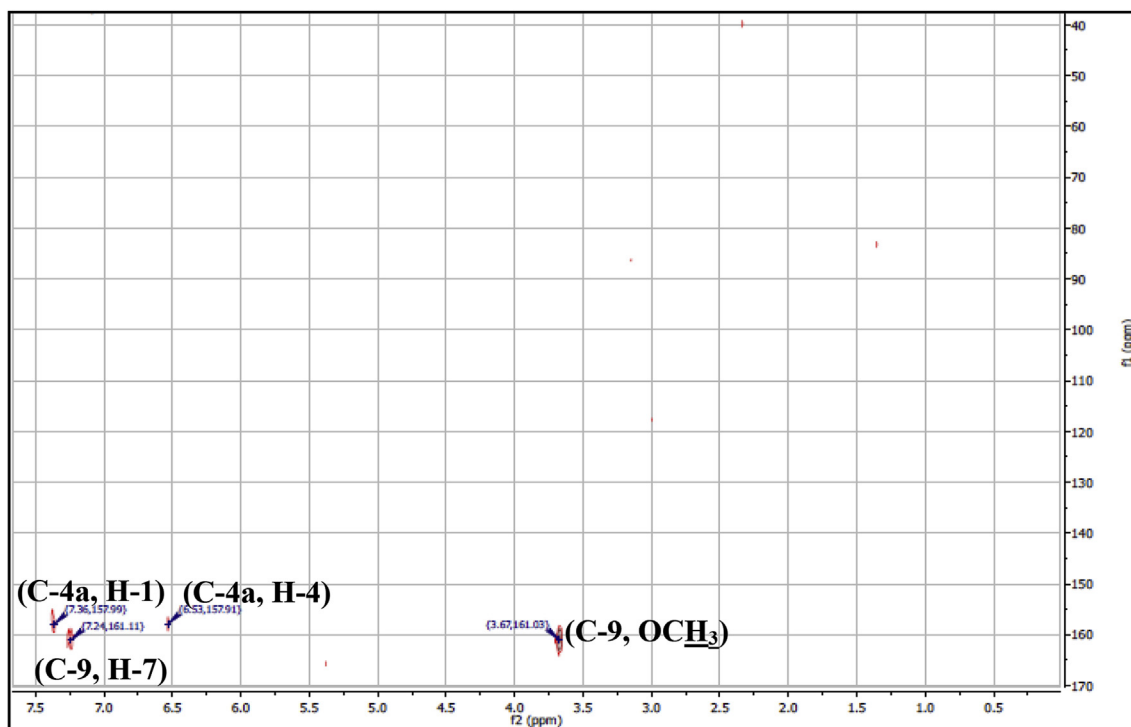


Fig. S29. HMBC spectrum of compound 6.

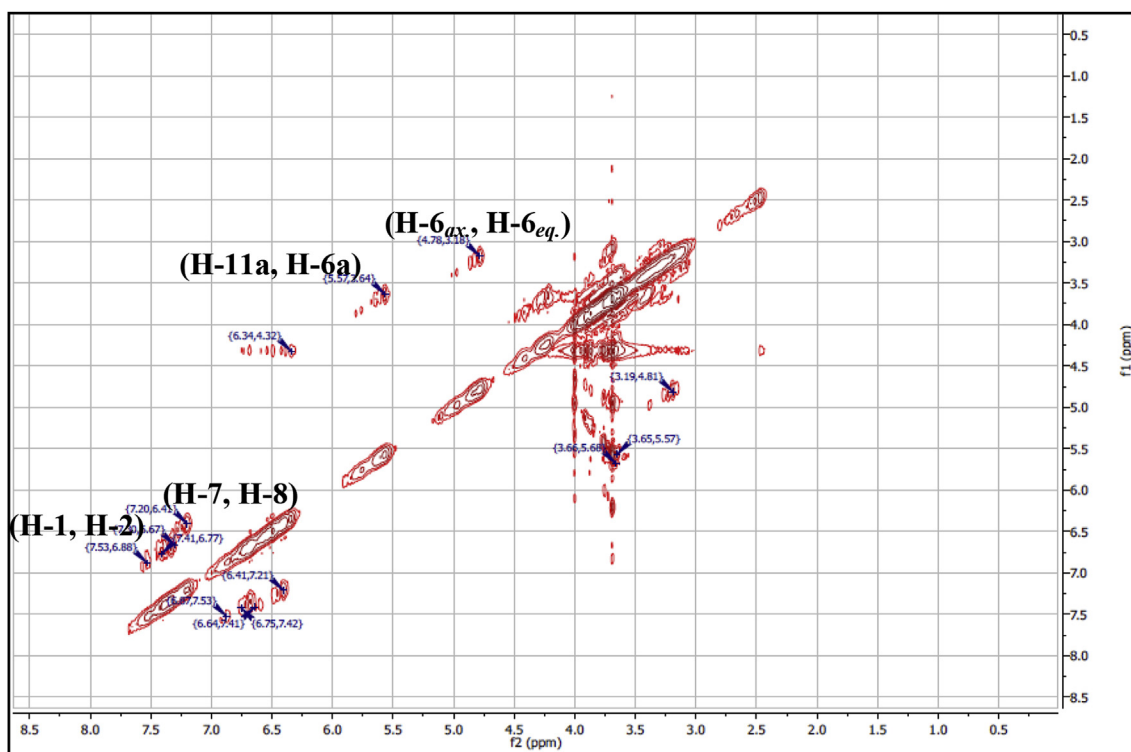


Fig. S30. COSY spectrum of compound 6.

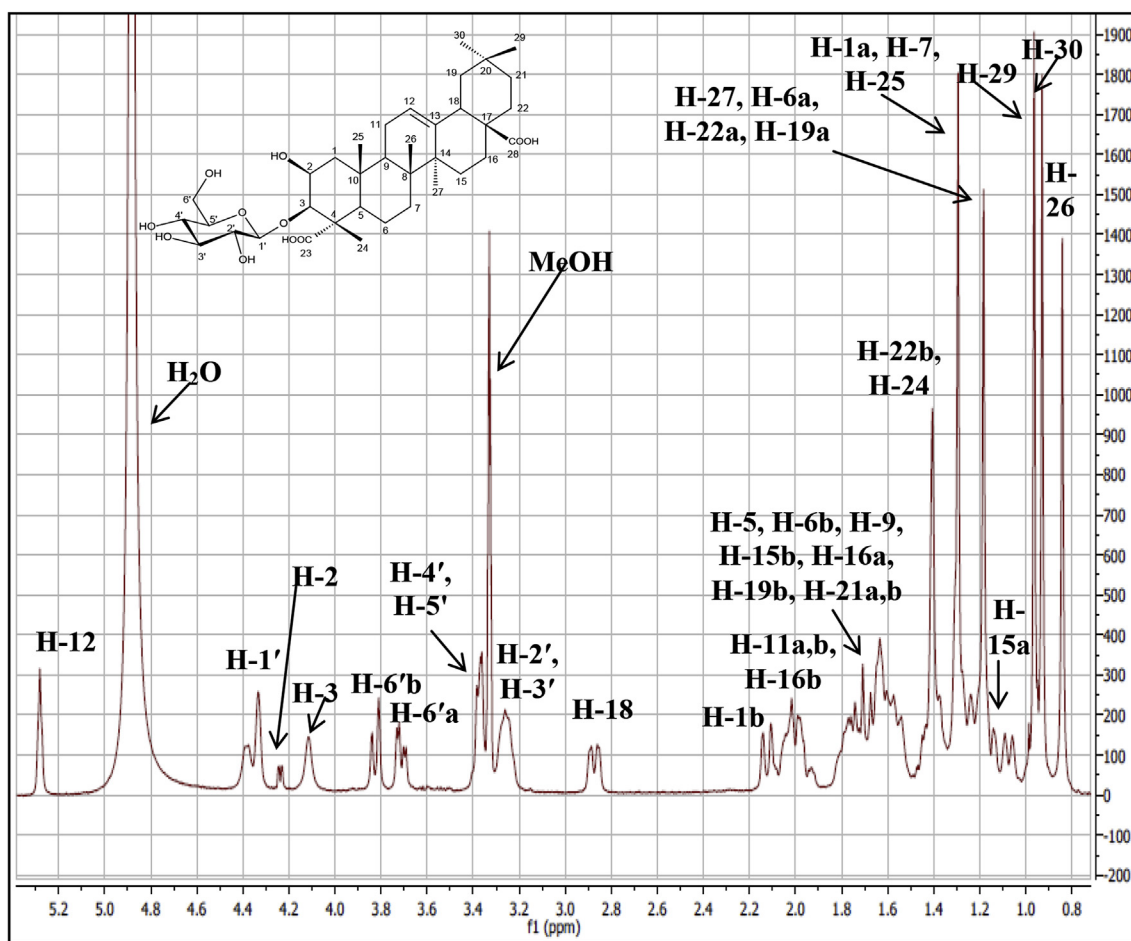


Fig. S31.  $^1\text{H}$  NMR (500 MHz) spectrum of compound 7 in  $\text{MeOH-}d_4$ .

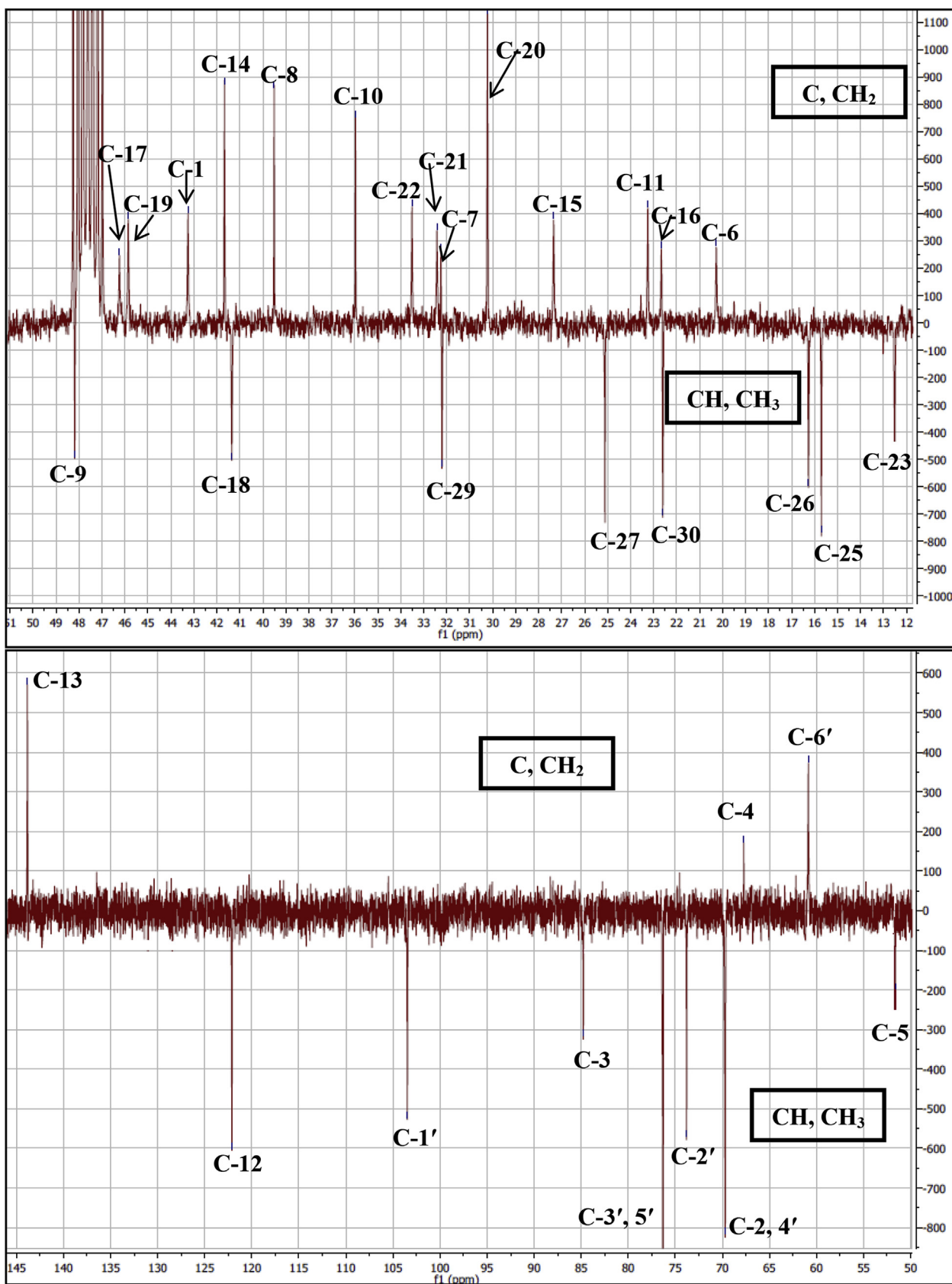


Fig. S32. APT spectrum of compound 7.

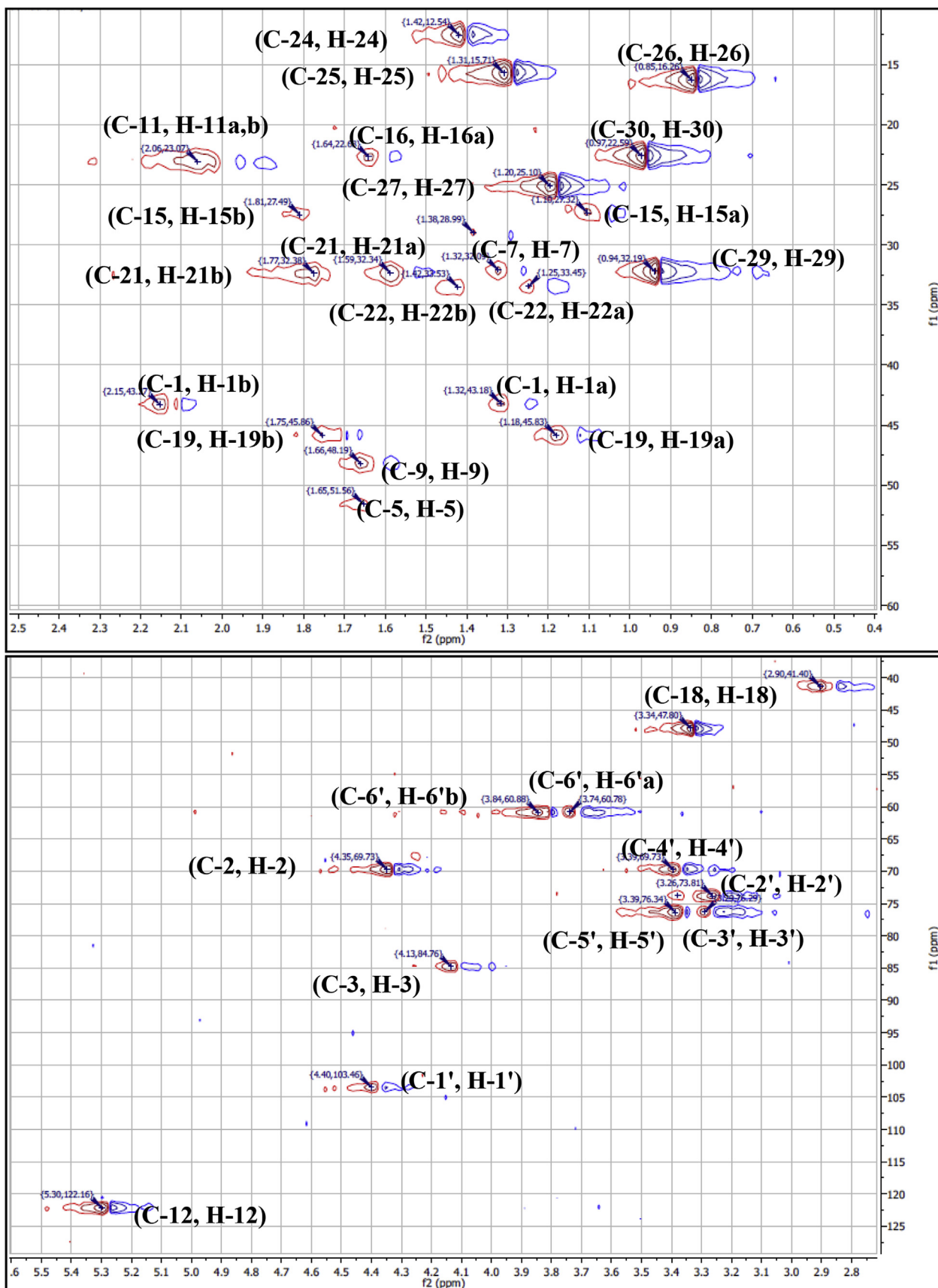


Fig. S33. HMQC spectrum of compound 7.

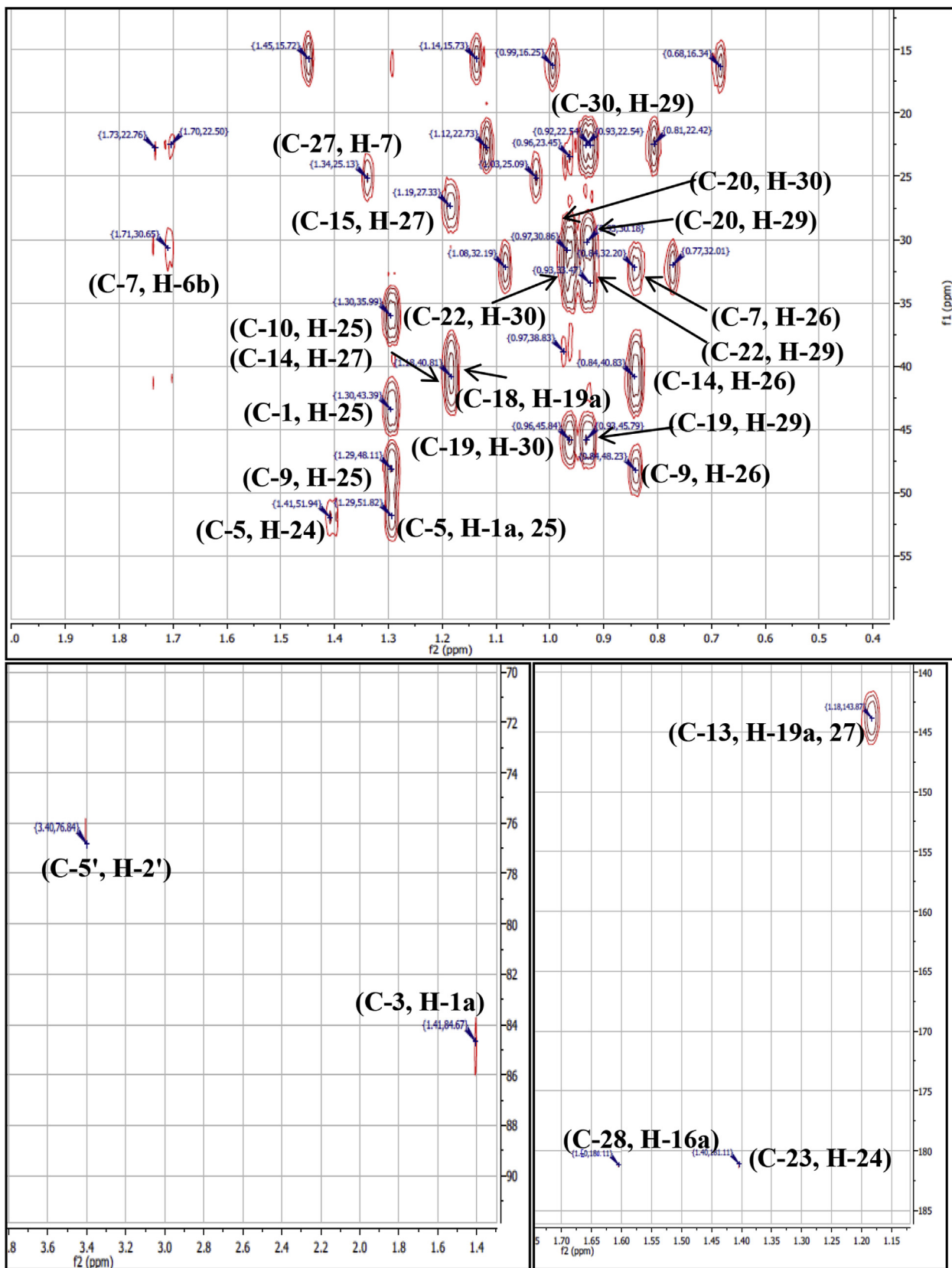


Fig. S34. HMBC spectrum of compound 7.

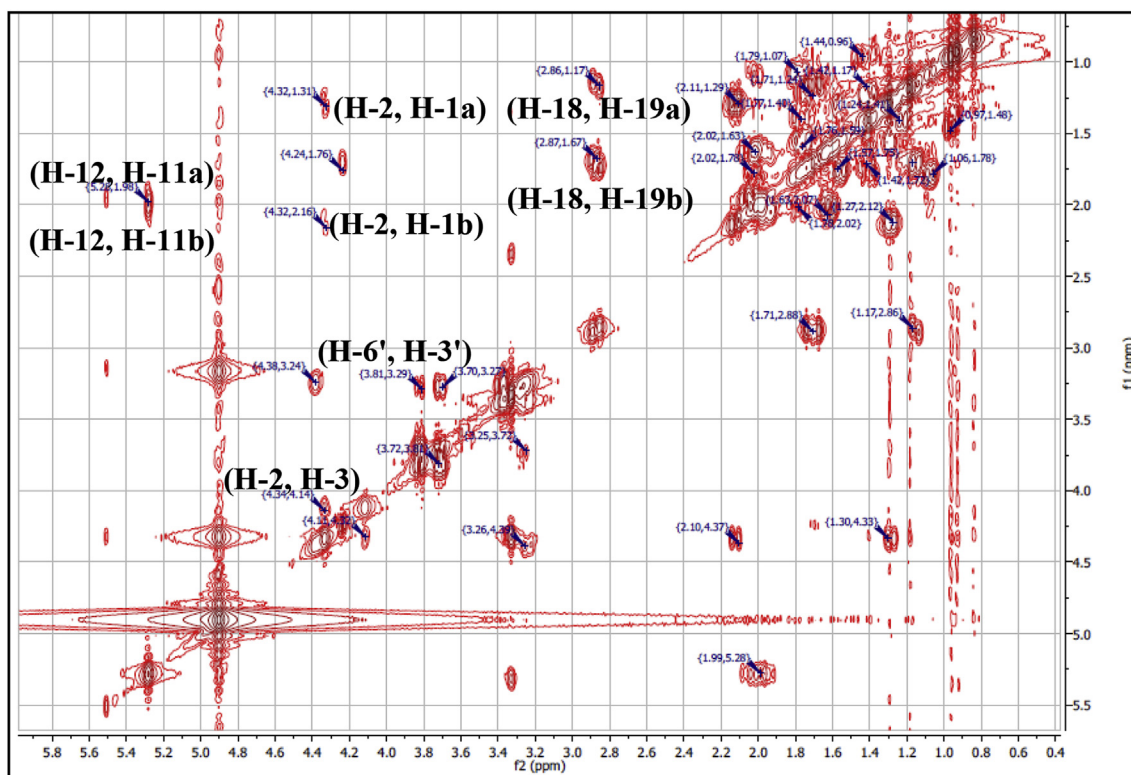


Fig. S35. COSY spectrum of compound 7.

Table 1.  $^1\text{H}$  and  $^{13}\text{C}$  NMR data of compounds 1 and 7

Position	1 (CDCl <sub>3</sub> )		7 (MeOH-d <sub>4</sub> )	
	$\delta_{\text{C}}$ (ppm)	$\delta_{\text{H}}$ (ppm) (int., mult., J (Hz))	$\delta_{\text{C}}$ (ppm)	$\delta_{\text{H}}$ (ppm) (int., mult., J (Hz))
1	37.15	1.09 (H-1a, m), 1.82 (H-1b, m)	43.26	1.30 (H-1a, m), 2.10 (H-1b, m)
2	31.49	1.39 (H-2a, m), 1.77 (H-2b, m)	69.75	4.30 (1H, dd, $J = 3.0, 4.0$ Hz)
3	71.07	3.61 (1H, m)	84.70	4.10 (1H, d, $J = 4.0$ Hz)
4	38.01	1.27 (H-4a, m), 1.70 (H-4b, m)	67.70	—
5	40.2	1.40 (1H, m)	51.62	1.60 (1H, m)
6	29.77	1.22 (H-6a, m), 1.74 (H-6b, m)	20.20	1.20 (H-6a, m), 70 (H-6b, m)
7	117.46	5.16 (1H, br s)	32.25	1.32 (1H, m)
8	139.50	—	39.51	—
9	49.46	1.65 (1H, m)	48.48	1.60 (1H, m)
10	34.20	—	35.90	—
11	21.56	1.48 (2H, m)	23.25	2.06 (H-11a, m), 2.16 (H-11b, m)
12	39.47	1.23 (H-12a, m), 2.02 (H-12b, m)	122.10	5.30 (1H, t, $J = 3.4$ Hz)
13	43.30	—	143.80	—
14	—	—	41.67	—
15	—	—	27.30	1.10 (H-15a, m), 1.80 (H-15b, m)
16	55.14	1.81 (1H, m)	22.66	1.60 (H-16a, m), 2.05 (H-16b, m)
17	22.98	1.40 (H-15a, m), 1.52 (H-15b, m)	46.24	—
18	28.52	1.25 (2H, m)	41.35	2.85 (1H, dd, $J = 3.0, 4.0$ Hz)
19	55.90	1.25 (1H, m)	45.85	1.16 (H-19a, m), 1.70 (H-19b, m)
20	12.00	0.57 (3H, s)	30.23	—
21	13.06	0.80 (3H, s)	32.43	1.59 (H-21a, m), 1.80 (H-21b, m)
22	40.84	2.05 (1H, m)	33.52	1.20 (H-22a, m), 1.40 (H-22b, m)
23	21.39	1.03 (3H, d, $J = 6.8$ Hz)	181.00	—
24	138.10	5.14 (1H, dd, $J = 8.8, 15.2$ Hz)	12.50	1.40 (3H, s)
25	129.4	5.02 (1H, dd, $J = 8.4, 15.2$ Hz)	15.70	1.30 (3H, s)
26	51.26	1.55 (1H, m)	16.20	0.84 (3H, s)
27	31.89	1.55 (1H, m)	25.10	1.18 (3H, s)
28	21.11	0.86 (3H, d, $J = 6.4$ Hz)	180.00	—
29	19.01	0.84 (3H, d, $J = 6.0$ Hz)	32.21	0.94 (3H, s)

(continued on next page)

Table 1. (continued)

Position	1 (CDCl <sub>3</sub> )		7 (MeOH-d <sub>4</sub> )	
	$\delta_C$ (ppm)	$\delta_H$ (ppm) (int., mult., J (Hz))	$\delta_C$ (ppm)	$\delta_H$ (ppm) (int., mult., J (Hz))
30			22.60 Glu	0.97 (3H, s)
1'			103.47	4.40 (d, J = 7.5 Hz, 1H)
2'			73.80	3.26 (1H, m)
3'			76.35	3.29 (1H, m)
4'			69.63	3.40 (1H, m)
5'			76.33	3.39 (1H, m)
6'			60.86	3.70 (H-6'a, m) 3.80 (H-6'b, m)

Int: integration of the NMR signal (showing the number of H); mult.: multiplicity of the NMR signal; J: coupling constant; s: singlet; bs: broad singlet; d: doublet; dd: doublet of doublet; m: multiplet.

Table 2. <sup>1</sup>H and <sup>13</sup>C NMR data of compounds 2, 4 and 5 in MeOH-d<sub>4</sub>

	2		4		5	
	$\delta_C$ (ppm)	$\delta_H$ (ppm)	$\delta_C$ (ppm)	$\delta_H$ (ppm)	$\delta_C$ (ppm)	$\delta_H$ (ppm)
2	79.62	(ax.) 5.4 (1H, dd, J = 13.1, 2.9 Hz)	164.53	—	167.05	—
3	43.56	(eq.) 2.71 (1H, dd, J = 16.9, 2.9 Hz) (ax.) 3.07 (1H, dd, J = 13.1, 16.9 Hz)	103.67	6.69 (1H, s)	102.45	6.61 (1H, s)
4	192.07	—	184.11	—	182.50	—
5	128.42	7.75 (1H, d, J = 8.7 Hz)	126.27	7.98 (1H, d, J = 8.7 Hz)	163.50	—
6	110.56	6.51 (1H, dd, J = 8.7, 2.2 Hz)	115.16	6.93 (1H, dd, J = 8.7, 2.1 Hz)	98.87	6.23 (1H, d, J = 2.1 Hz)
7	164.11	—	161.29	—	165.03	—
8	102.47	6.36 (1H, d, J = 2.2 Hz)	102.15	6.97 (1H, d, J = 2.1 Hz)	93.75	6.48 (1H, d, J = 2.1 Hz)
9	169.90	—	160.12	—	159.50	—
10	113.70	—	117.17	—	105.30	—
1'	129.98	—	125.11	—	121.98	—
2',6'	127.59	7.38 (2H, d, J = 8.6 Hz)	127.95	7.9 (2H, d, J = 8.9 Hz)	128.07	7.88 (2H, d, J = 8 Hz)
3',5'	114.90	6.88 (2H, d, J = 8.6 Hz)	115.62	6.95 (2H, d, J = 8.9 Hz)	115.76	6.95 (2H, d, J = 8 Hz)
4'	159.00	—	162.01	—	161.34	—

Int: integration of the NMR signal (showing the number of H); mult.: multiplicity of the NMR signal; J: coupling constant; d: doublet; dd: doublet of doublet.

Table 3. <sup>1</sup>H and <sup>13</sup>C NMR data of compound 3 in DMSO-d<sub>6</sub>

	$\delta_C$ (ppm)	$\delta_H$ (ppm) (int., mult., J (Hz))
1	126.22	—
2,6	131.65	7.78 (2H, d, J = 8.5 Hz)
3,5	116.31	6.84 (2H, d, J = 8.5 Hz)
4	160.74	—
$\alpha$	117.91	7.76 (1H, d, J = 15.4 Hz)
$\beta$	144.60	7.77(1H, d, J = 15.4 Hz)
$\beta'$	191.89	—
1'	114.20	—
2'	166.29	—
3'	103.07	6.26 (1H, d, J = 2.1 Hz)
4'	167.50	—
5'	108.75	6.39 (1H, dd, J = 8.9, 2.1 Hz)
6'	133.27	8.15 (1H, d, J = 8.9 Hz)
2' -OH	—	13.67 (1H, s)

Int: integration of the NMR signal (showing the number of H); mult.: multiplicity of the NMR signal; J: coupling constant; s: singlet; d: doublet; dd: doublet of doublet.

Table 4. <sup>1</sup>H and <sup>13</sup>C NMR data of compound 6 in DMSO-d<sub>6</sub>

	$\delta_C$ (ppm)	$\delta_H$ (ppm) (int., mult., J (Hz))
1	132.45	7.38 (1H, d, J = 8.3 Hz)
2	110.89	6.72 (1H, dd, J = 8.3 Hz, 2.5 Hz)
3	160.61	—
4	104.43	6.54 (1H, d, 2.5 Hz)
4a	158.80	—
6	66.39	3.73 (1H, dd, J = 11.0, 11.0 Hz, H-6 <sub>ax</sub> )
$\beta'$	191.89	4.27 (1H, dd, J = 11.0, 5.0 Hz, H-6 <sub>eq</sub> )
6a	40.20	3.59 (1H, ddd, J = 11.0, 7.0, 5.0 Hz)
6b	119.61	—
7	125.69	7.24 (1H, d, J = 8.1 Hz)
8	106.61	6.45 (1H, dd, J = 8.1, 2.5 Hz)
9	161.58	—
10	96.72	6.40 (1H, d, J = 2.5 Hz)
10a	160.97	—
11a	78.21	5.60 (1H, d, J = 7.0 Hz)
11b	114.79	—
OCH <sub>3</sub>	55.74	3.69 (3H, s)
1'	100.62	4.80 (1H, d, J = 7.4 Hz)
2'	73.41	3.10–3.27 (4H, m)
3'	76.60	—
4'	69.96	—
5'	77.27	—
6'	60.95	3.30 (H-6'a, m)

Int: integration of the NMR signal (showing the number of H); mult.: multiplicity of the NMR signal; J: coupling constant; s: singlet; d: doublet; dd: doublet of doublet; m: multiplet.

## References

- [1] Taylor PN, Albrecht D, Scholz A, Gutierrez-Buey G, Lazarus JH, Dayan CM, Okosieme OE. Global epidemiology of hyperthyroidism and hypothyroidism. *Nat Rev Endocrinol* 2018;14:301–16.
- [2] Biondi B, Bartalena L, Cooper DS, Hegedüs L, Laurberg P, Kahaly GJ. The 2015 European Thyroid Association guidelines on diagnosis and treatment of endogenous subclinical hyperthyroidism. *Eur Thyroid J* 2015;4:149–63.
- [3] Bianco AC, Salvatore D, Gereben B, Berry MJ, Larsen PR. Biochemistry, cellular and molecular biology, and physiological roles of the iodothyronine selenodeiodinases. *Endocr Rev* 2002;23:38–89.
- [4] Cooper DS. Antithyroid drugs. *N Engl J Med* 2005;352:905–17.
- [5] Bahn Chair RS, Burch HB, Cooper DS, Garber JR, Greenlee MC, Klein I, Laurberg P, McDougall IR, Montori VM, Rivkees SA, Ross DS, Sosa JA, Stan MN. Hyperthyroidism and other causes of thyrotoxicosis: management guidelines of the American Thyroid Association and American Association of Clinical Endocrinologists. *Thyroid* 2011;21:593–646.
- [6] Warnock AL, Cooper DS, Burch HB. Life-threatening thyrotoxicosis: Thyroid storm and adverse effects of antithyroid drugs. In: Maffin G, editor. *Endocrine and metabolic medical emergencies: A clinician's guide*. Washington: Endocrine Society/Endocrine Press; 2018. p. 262–83.
- [7] Doige CE, McLaughlin BG. Hyperplastic goitre in newborn foals in Western Canada. *Can Vet J* 1981;22:42–5.
- [8] Kreplin C, Allen A. Alberta. Congenital hypothyroidism in foals in Alberta. *Can Vet J* 1991;32:751.
- [9] Allen AL, Doige CE, Fretz PB, Townsend HG. Hyperplasia of the thyroid gland and concurrent musculoskeletal deformities in western Canadian foals: reexamination of a previously described syndrome. *Can Vet J* 1994;35:31.
- [10] Allen AL, Townsend HG, Doige CE, Fretz PB. A case-control study of the congenital hypothyroidism and dysmaturity syndrome of foals. *Can Vet J* 1996;37:349–51.
- [11] Allen A. Congenital hypothyroidism in foals. *Can Vet J* 2001;42:418.
- [12] Gawrylash SK. Thyroid hyperplasia and musculoskeletal deformity in a standardbred filly in Ontario. *Can Vet J* 2004;45:424–6.
- [13] Koikkalainen K, Knuutila A, Karikoski N, Syrjä P, Hewetson M. Congenital hypothyroidism and dysmaturity syndrome in foals: First reported cases in Europe. *Equine Vet Educ* 2014;26:181–9.
- [14] Rafińska K, Pomastowski P, Wrona O, Górecki R, Buszewski B. *Medicago sativa* as a source of secondary metabolites for agriculture and pharmaceutical industry. *Phytochem Lett* 2017;20:520–39.
- [15] Gaweł E, Grzelak M, Janyszek M. Lucerne (*Medicago sativa* L.) in the human diet-Case reports and short reports. *J Herb Med* 2017;10:8–16.
- [16] Mir SA, Shah MA, Mir MM. Microgreens: Production, shelf life, and bioactive components. *Crit Rev Food Sci Nutr* 2017;57:2730–6.
- [17] Benincasa P, Falcinelli B, Lutts S, Stagnari F, Galieni A. Sprouted grains: A comprehensive review. *Nutrients* 2019;11:421.
- [18] Hong Y-H, Chao W-W, Chen M-L, Lin B-F. Ethyl acetate extracts of alfalfa (*Medicago sativa* L.) sprouts inhibit lipopolysaccharide-induced inflammation *in vitro* and *in vivo*. *J Biomed Sci* 2009;16:64.
- [19] Oh MM, Rajashekar CB. Antioxidant content of edible sprouts: effects of environmental shocks. *J Sci Food Agric* 2009;89:2221–7.
- [20] Mattioli S, Dal Bosco A, Martino M, Ruggeri S, Marconi O, Sileoni V, Falcinelli B, Castellini B, Benincasa P. Alfalfa and flax sprouts supplementation enriches the content of bioactive compounds and lowers the cholesterol in hen egg. *J Funct Foods* 2016;22:454–62.
- [21] Ibrahim RS, Khairy A, Zaatout HH, Hammada HM, Metwally AM. Digitally-optimized HPTLC coupled with image analysis for pursuing polyphenolic and antioxidant profile during alfalfa sprouting. *J Chromatogr B* 2018;1099:92–6.
- [22] Pedersen MW. Relative quantity and biological activity of saponins in germinated seeds, roots, and foliage of Alfalfa 1. *Crop Sci* 1975;15:541–3.
- [23] Council NR. Guide for the care and use of laboratory animals. Institute of Laboratory Animal Resources, Commission on Life Sciences. Washington DC: National Academy of Sciences; 1996.
- [24] Dong H, Godlewska M, Wade MG. A rapid assay of human thyroid peroxidase activity. *Toxicol In Vitro* 2020;62:104662.
- [25] Schweizer U, Schlicker C, Braun D, Köhrle J, Steegborn C. Crystal structure of mammalian selenocysteine-dependent iodothyronine deiodinase suggests a peroxiredoxin-like catalytic mechanism. *Proc Natl Acad Sci* 2014;111:10526–31.
- [26] Kampmann JP, Hansen JM. Clinical pharmacokinetics of antithyroid drugs. *Clin Pharmacokinet* 1981;6:401–28.
- [27] Bhaigiyabati T, Ramya J, Usha K. Effect of methanolic extract of sweet corn silk on experimentally induced hyperthyroidism in Swiss albino rats. *Int Res J Pharm* 2012;3:241–5.
- [28] Kim SM, Kim SC, Chung IK, Cheon WH, Ku SK. Antioxidant and protective effects of bupleurum falcatum on the L-thyroxine-induced hyperthyroidism in rats. *Evid. Based. Complement. Alternat Med* 2012;578497:25.
- [29] Bustin SA, Benes V, Garson JA, Hellems J, Huggett J, Kubista M, Mueller R, Nolan T, Pfaffl MW, Shipley GL, Vandesompele J, Wittwer CT. The MIQE guidelines: minimum information for publication of quantitative real-time PCR experiments. *Clin Chem* 2009;55:611–22.
- [30] Tuuminen T. Fluorometric enzyme immunoassay for the determination of thyroxine from dried blood spots. *Screen* 1993;2:149–58.
- [31] Bucolo G, David H. Quantitative determination of serum triglycerides by the use of enzymes. *Clin Chem* 1973;19:476–82.
- [32] Allain CC, Poon LS, Chan CSG, Richmond W, Fu PC. Enzymatic determination of total serum cholesterol. *Clin Chem* 1974;20:470–5.
- [33] Grove TH. Effect of reagent pH on determination of high-density lipoprotein cholesterol by precipitation with sodium phosphotungstate-magnesium. *Clin Chem* 1979;25:560–4.
- [34] Hu LW, Benvenuti LA, Liberti EA, Carneiro-Ramos MS, Barreto-Chaves ML. Thyroxine-induced cardiac hypertrophy: influence of adrenergic nervous system versus renin-angiotensin system on myocyte remodeling. *Am J Physiol Regul Integr Comp Physiol* 2003;285:R1473–80.
- [35] El-Mezayen NS, El-Hadidy WF, El-Refaie WM, Shalaby TI, Khattab MM, El-Khatib AS. Oral vitamin-A-coupled valsartan nanomedicine: High hepatic stellate cell receptors accessibility and prolonged enterohepatic residence. *J Control Release* 2018;283:32–44.
- [36] Reitman S, Frankel S. A colorimetric method for the determination of serum glutamic oxalacetic and glutamic pyruvic transaminases. *Am J Clin Pathology* 1957;28:56–63.
- [37] Kirkpatrick LA, Feeney BC. A simple guide to IBM SPSS: for version 20.0. Toronto: Nelson Education; 2012.
- [38] Cavanaugh J. Encyclopedia of statistical sciences. In: 2nd ed. Kotz Samuel, Read Campbell B, Balakrishnan N, Vidakovic Brani, editors. Vol. 102; 2007. p. 1074–93. J Am Stat Assoc.
- [39] Villaseñor IM, Lemon P, Palileo A, Bremner JB. Antigenotoxic spinasterol from Cucurbita maxima flowers. *Mutat Res Genet Toxicol Environ Mutagen* 1996;360:89–93.
- [40] Villaseñor IM, Domingo AP. Anticarcinogenicity potential of spinasterol isolated from squash flowers. *Teratog Carcinog Mutagen* 2000;20:99–105.

- [41] Ma C-j, Li G-s, Zhang D-l, Liu K, Fan X. One step isolation and purification of liquiritigenin and isoliquiritigenin from *Glycyrrhiza uralensis* Risch. using high-speed counter-current chromatography. *J Chromatogr A* 2005;1078:188–92.
- [42] Hong Y-H, Wang S-c, Hsu C, Lin B-F, Kuo Y-H, Huang C-j. Phytoestrogenic compounds in alfalfa sprout (*Medicago sativa*) beyond coumestrol. *J Agr Food Chem* 2010;59:131–7.
- [43] Khamsan S, Liawruangrath S, Teerawutkulrag A, Pyne S, Garson M, Liawruangrath B. The isolation of bioactive flavonoids from *Jacaranda obtusifolia* HBK ssp. *rhombifolia* (GFW Meijer) Gentry. *Acta Pharm* 2012;62:181–90.
- [44] Carvalho MGd, Gomes MSR, de Oliveira MCC, Silva Cjd, Carvalho AGd. Chemical constituents from *Piptadenia rigida* Benth., Fabaceae, "angico". *Rev Bras Farmacogn* 2011;21:397–401.
- [45] Van Loo P, De Bruyn A, Buděšínský M. Reinvestigation of the structural assignment of signals in the <sup>1</sup>H and <sup>13</sup>C NMR spectra of the flavone apigenin. *Magn Reson Chem* 1986;24:879–82.
- [46] Sakagami Y, Kumai S, Suzuki A. Isolation and structure of medicarpin-β-d-glucoside in alfalfa. *Agric Biol Chem* 1974;38:1031–4.
- [47] Oleszek W, Price KR, Colquhoun IJ, Jurzysta M, Ploszynski M, Fenwick GR. Isolation and identification of alfalfa (*Medicago sativa* L.) root saponins: their activity in relation to a fungal bioassay. *J Agric Food Chem* 1990;38:1810–7.
- [48] Sharma S, Singh AK, Kaushik S, Sinha M, Singh RP, Sharma P, Sirohi H, Kaur P, Singh TP. Lactoperoxidase: structural insights into the function, ligand binding and inhibition. *Int J Biochem Mol Biol* 2013;4:108–28.
- [49] Singh RP, Singh A, Sirohi HV, Singh AK, Kaur P, Sharma S, Singh TP. Dual binding mode of antithyroid drug methimazole to mammalian heme peroxidases—structural determination of the lactoperoxidase–methimazole complex at 1.97 Å resolution. *FEBS Open Bio* 2016;6:640–50.
- [50] Gradolatto A, Basly JP, Berges R, Teyssier C, Chagnon MC, Siess MH, Canivenc-Lavier MC. Pharmacokinetics and metabolism of apigenin in female and male rats after a single oral administration. *Drug Metab Dispos* 2005;33:49–54.
- [51] Gérard A-C, Deneff J-F, Colin IM, van den Hove M-F. Evidence for processing of compact insoluble thyroglobulin globules in relation with follicular cell functional activity in the human and the mouse thyroid. *Eur J Endocr* 2004;150:73–80.
- [52] Lee J, Yi S, Kang YE, Kim H-W, Joung KH, Sul HJ, Kim KS, Shong M. Morphological and functional changes in the thyroid follicles of the aged murine and humans. *J Pathol. Transl Med* 2016;50:426–35.
- [53] Sellers EA, Hill JM, Lee RB. Effect of iodide and thyroid on the production of tumors of the thyroid and pituitary by propylthiouracil. *Endocrinol* 1953;52:188–203.
- [54] Cachefo ANA, Boucher P, Vidon C, Dusserre E, Fdr Diraison, Beylot M. Hepatic lipogenesis and cholesterol synthesis in hyperthyroid patients. *J Clin Endocrinol Metab* 2001;86:5353–7.
- [55] Altaher WH, Ahemd EM, Ismail A. Assessment of lipids profile in hyperthyroidism Sudanese patients in North Kordofan State. Sudan. *J Sci Technol* 2013;14:1–7.
- [56] Hansson P, Valdemarsson S, Nilsson-Ehle P. Experimental hyperthyroidism in man: effects on plasma lipoproteins, lipoprotein lipase and hepatic lipase. *Horm Metab Res* 1983;15:449–52.
- [57] Rizos CV, Elisaf MS, Liberopoulos EN. Effects of thyroid dysfunction on lipid profile. *Open Cardiovasc Med J* 2011;5:76–84.
- [58] Chen Y, Wu X, Wu R, Sun X, Yang B, Wang Y, Xu Y. Changes in profile of lipids and adipokines in patients with newly diagnosed hypothyroidism and hyperthyroidism. *Sci Rep* 2016;6:26174.
- [59] Aviram M, Luboshitzky R, Brook JG. Lipid and lipoprotein pattern in thyroid dysfunction and the effect of therapy. *Clin Biochem* 1982;15:62–6.
- [60] Laurberg P, Tørring J, Weeke J. A comparison of the effects of propylthiouracil and methimazol on circulating thyroid hormones and various measures of peripheral thyroid hormone effects in thyrotoxic patients. *Eur J Endocrinol* 1985;108:51–4.
- [61] Jung U, Cho Y-Y, Choi M-S. Apigenin ameliorates dyslipidemia, hepatic steatosis and insulin resistance by modulating metabolic and transcriptional profiles in the liver of high-fat diet-induced obese mice. *Nutrients* 2016;8:305.
- [62] Ren B, Qin W, Wu F, Wang S, Pan C, Wang L, Zeng B, Ma S, Liang J. Apigenin and naringenin regulate glucose and lipid metabolism, and ameliorate vascular dysfunction in type 2 diabetic rats. *Eur J Pharmacol* 2016;773:13–23.
- [63] Dorr M, Wolff B, Robinson DM, John U, Ludemann J, Meng W, Volzke H. The association of thyroid function with cardiac mass and left ventricular hypertrophy. *J Clin Endocrinol Metab* 2005;90:673–7.
- [64] Fadel BM, Ellahham S, Lindsay J, Ringel MD, Wartofsky L, Burman KD. Hyperthyroid heart disease. *Clin Cardiol* 2000;23:402–8.
- [65] Dillmann W. Cardiac hypertrophy and thyroid hormone signaling. *Heart Fail Rev* 2010;15:125–32.
- [66] Klein I, Danzi S. Thyroid disease and the heart. *Circulation* 2007;116:1725–35.
- [67] Kotajima N, Yanagawa Y, Aoki T, Tsunekawa K, Morimura T, Ogiwara T, Murakami M. Influence of thyroid hormones and transforming growth factor-β1 on cystatin C concentrations. *J Int Med Res* 2010;38:1365–73.
- [68] Hajje G, Saliba Y, Itani T, Moubarak M, Aftimos G, Farès N. Hypothyroidism and its rapid correction alter cardiac remodeling. *PloS one* 2014;9:e109753.
- [69] Saad NS, Repas SJ, Floyd K, Janssen PML, Elnakish MT. Recovery following thyroxine treatment withdrawal, but not propylthiouracil, averts *in vivo* and *ex vivo* thyroxine-provoked cardiac complications in adult FVB/N mice. *Biomed Res Int* 2017;2017:1–11.
- [70] Chopra IJ, Huang T-S, Hurd RE, Solomon DH. A study of cardiac effects of thyroid hormones: evidence for amelioration of the effects of thyroxine by sodium ipodate. *Endocrinol* 1984;114:2039–45.
- [71] Osman F, Franklyn JA, Holder RL, Sheppard MC, Gammage MD. Cardiovascular manifestations of hyperthyroidism before and after antithyroid therapy: a matched case-control study. *J Am Coll Cardiol* 2007;49:71–81.
- [72] Kisso B, Patel A, Redetzke R, Gerdes AM. Effect of low thyroid function on cardiac structure and function in spontaneously hypertensive heart failure rats. *J Card Fail* 2008;14:167–71.
- [73] Buwa CC, Mahajan UB, Patil CR, Goyal SN. Apigenin attenuates β-receptor-stimulated myocardial injury via safeguarding cardiac functions and escalation of antioxidant defence system. *Cardiovasc. Toxicol* 2016;16:286–97.
- [74] Zhu Z-Y, Gao T, Huang Y, Xue J, Xie M-L. Apigenin ameliorates hypertension-induced cardiac hypertrophy and down-regulates cardiac hypoxia inducible factor-1α in rats. *Food Funct* 2016;7:1992–8.
- [75] Liu H-J, Fan Y-L, Liao H-H, Liu Y, Chen S, Ma Z-G, Zhang N, Yang Z, Deng W, Tang Q-Z. Apigenin alleviates STZ-induced diabetic cardiomyopathy. *Mol Cell Biochem* 2017;428:9–21.
- [76] Madani SH, Far ZR, Jalilian N, Zare ME, Zadeh FS. Evaluate the liver function in hyperthyroidism patients. *J Paramed Sci* 2014;5:1–4.
- [77] Upadhyay G, Singh R, Kumar A, Kumar S, Kapoor A, Godbole MM. Severe hyperthyroidism induces mitochondria-mediated apoptosis in rat liver. *Hepatology* 2004;39:1120–30.
- [78] Zeng X, Zhan L, Zhao Y. Exploration and analysis of the effect of thiamazole and propylthiouracil on serum glutamic pyruvic transaminase and serum bilirubin level as well as liver damage incidence in patients with hyperthyroidism. *Int J Clin Exp Med* 2018;11:2642–7.

- [79] Jamshidzadeh A, Niknahad H, Heidari R, Azadbakht M, Khodaei F, Arabnezhad MR, Farshad O. Propylthiouracil-induced mitochondrial dysfunction in liver and its relevance to drug-induced hepatotoxicity. *Pharm Sci* 2017;23:95–102.
- [80] Wang F, Liu J-C, Zhou R-J, Zhao X, Liu M, Ye H, Xie M-L. Apigenin protects against alcohol-induced liver injury in mice by regulating hepatic CYP2E1-mediated oxidative stress and PPAR $\alpha$ -mediated lipogenic gene expression. *Chem Biol Interact* 2017;275:171–7.
- [81] Zhou RJ, Ye H, Wang F, Wang JL, Xie ML. Apigenin inhibits d-galactosamine/LPS-induced liver injury through upregulation of hepatic Nrf-2 and PPAR $\gamma$  expressions in mice. *Biochem Biophys Res Commun* 2017;493:625–60.
- [82] Dorgalaleh A, Mahmoodi M, Varmaghani B. Effect of thyroid dysfunctions on blood cell count and red blood cell indice. *Iran J Pediatr Hematol Oncol* 2013;3:73–7.
- [83] Degerli V, Yilmaz Duran F, Kucuk M, Atasoy I. A rare cause of neutropenic enterocolitis: Propylthiouracil-induced agranulocytosis. *Hong Kong J Emerg Med* 2018;25:286–9.
- [84] Meng S, Zhu Y, Li J-F, Wang X, Liang Z, Li S-Q, Xu X, Chen H, Liu B, Zheng X-Y. Apigenin inhibits renal cell carcinoma cell proliferation. *Oncotarget* 2017;8:19834–42.
- [85] Raj P, Azamthulla M, Anbu J, Balaji R, Kumar S. Evaluation of anticancer activity of apigenin alone and combination with imatinib in SCID mice bearing K562 disseminated leukemic model. *J Chem Pharm Sci* 2017;10:111–20.